Northumbria Research Link

Northumbria
University
NEWCASTLE

Joint Dimming Control and Optimal Power Allocation for THO-OFDM Visible Light Communications

Han Ji, Tian Zhang, Shuang Qiao, and Zabih Ghassemlooy, *Senior Member, IEEE*

***Abstract*—Layered or hybrid optical orthogonal frequency division multiplexing (OFDM) has been proposed for use in optical communications due to its excellent spectral and power efficiencies, especially in visible light communications (VLC). However, most of the current works concentrate on transmitter and receiver design as well as the quality of service in communication networks. In this paper, we propose a spectrum-efficient dimmable triple-layer hybrid optical OFDM (DTH-OFDM) scheme to tackle the illumination requirements, considering different practical indoor VLC scenarios from low illumination to high illumination intensities. In the proposed DTH-OFDM scheme, the required dimming level is achieved by jointly adjusting the dimming factors and direct current bias. We investigate the comprehensive performance analysis of the proposed DTH-OFDM in detail, including probability density function, bit error rate (BER), spectral and energy efficiencies. In addition, a joint dimming control and optimal power allocation problem for DTH-OFDM is formulated and solved using convex optimization under the constraints of light emitting diode (LED) nonlinearity, dimming target and communications reliability. Numerical results show that, the proposed DTH-OFDM can offer continuous and arbitrary dimming target with higher spectral efficiency and lower BER compared with its counterparts, as well as an enhanced tolerance to the LED nonlinearity.**

***Index Terms*—Orthogonal frequency division multiplexing (OFDM), dimming control, power allocation, convex optimization, visible light communication.**

I. Introduction

The exponential growth in the data capacity and the demand for access to the transmission bandwidth usage has aggravated the shortage of radio-frequency (RF) spectrums, which will get more challenging in the fifth generation (5G) and the future sixth generation (6G) wireless communication networks [1]. One possible option to address this problem has been to shift to the terahertz (THz) of 10 THz [2], [3], which comes with its own challenges of power consumption, complexity and cost of the devices including the sources, power amplifiers, antennas and subharmonic mixers. Alternatively, the free visible spectrum (380 - 780 THz) could be adopted to provide visible light communications (VLC) using the energy efficient light-emitting diodes (LEDs)-based lighting fixtures in indoor and to some extend outdoor environments, thus alleviating the ongoing pressure on the RF-based wireless technologies [1, 4-6]. In fact, in most indoor environments visible and infrared wireless communications could be the most viable technology offering illumination, data communications, localization and sending, which are low cost with high security and immunity to RF electromagnetic interference, compared with RF systems [7], [8].

A. Related Works

Intensity modulation/direct detection (IM/DD) VLC systems are the most widely used and reported in the literature [9], e.g., (i) baseband and single carrier modulations such as on and off keying (OOK), pulse amplitude modulation (PAM), and pulse position modulation (PPM) [10], [11]; (ii) polarisation-division multiplexing, which offer increased spectral efficiency (SE) [12], and (iii) multi-level and -carrier modulation schemes including orthogonal frequency division multiplexing (OFDM) also known as discrete multitone (DMT) [13], [14], multi-band carrier-less amplitude and phase [15] and non-orthogonal multiple access [16], which offer higher SE and immunity to the multipath-induced inter-symbol interference (ISI). Among these, the most widely investigated scheme is OFDM and its variants of direct current (DC) biased optical OFDM (DCO-OFDM) [17], asymmetrically clipped optical OFDM (ACO-OFDM) [18], and PAM-DMT [19]. DCO-OFDM offer low energy efficiency (EE) due to the bias power, whereas ACO-OFDM and PAM-DMT suffer from reduced SE due to not utilizing half the spectrum. In addition, to improve the SE other schemes such as (i) hybrid schemes have been proposed including asymmetrically clipped DC biased O-OFDM (ADO-OFDM) [20], hybrid asymmetrically clipped OFDM (HACO-OFDM) [21], asymmetrically clipped absolute value optical OFDM (AAO-OFDM) [22], hybrid PAM-DMT (HPAM-DMT) [23], and polarization OFDM [24] have been proposed to improve the SE; And (ii) layered (or enhanced) schemes including enhanced U-OFDM (eU-OFDM) [25], layered ACO-OFDM (LACO-OFDM) [26], absolute value layered ACO-OFDM (ALACO-OFDM) [27] and augmented SE-DMT (ASE-DMT) [28], where infinite layer unipolar U-OFDM, ACO-OFDM or PAM-DMT can be superimposed. Superior to the layered/enhanced schemes with infinite layers superimposition, a triple-layer hybrid optical OFDM (THO-OFDM) scheme reaching the SE limit of LACO-OFDM was

This work was supported in part by the Foundation for Excellent Young Talents of Jilin Province under Grant 20190103010JH, and in part by the National Natural Science Foundation of China under Grant 11905028.*(Corresponding author: Tian Zhang.)*

H. Ji, T. Zhang and S. Qiao are with School of Physics, Northeast Normal University, Changchun 130024, China (e-mail:{jih066, zhangt100}@nenu.edu.cn).

Z. Ghassemlooy is with Optical Communications Research Group, Faculty of Engineering and Environment, Northumbria University, Newcastle upon Tyne NE1 8ST, U.K.

proposed with enhanced performance and reduced computation complexity [14], [29].

In VLC system, which offers simultaneous data communications and illumination, dimming is identified as one of the key challenges in the IEEE 802.15.7 standard that needs further investigation [30], [31]. In single carrier modulation-based VLC, dimming control is usually achieved using OOK, PAM, pulse width modulation (PWM) and PPM [32-34]. In OFDM-based VLC systems, a number of dimming control schemes have been investigated including (i) adjusting the DC bias in DCO-OFDM, where at the low (or high) dimming level the system performance is limited due to the LED nonlinearity [35], which is further investigated using a piecewise function [36]; and (ii) reverse polarity optical-OFDM (RPO-OFDM) with dimming [37], where PWM is combined with the ACO-OFDM during the "On" and "Off" stages for full utilization of the PWM full cycle. To achieve higher SE and a flexible dimming range, several hybrid or layered dimming schemes have been proposed. In [38], asymmetrical hybrid optical OFDM (AHO-OFDM) with adjustable DC bias and modulation orders was investigated by combing ACO-OFDM and reverse PAM-DMT signals in the odd and even subcarriers (SCs). In [39], dimmable optical OFDM (DO-OFDM), which is an improved version of LACO-OFDM, was proposed where different dimming levels were attained by adjusting the scaling factors, modulation order and DC bias. The negative HACO-OFDM (NHACO-OFDM) [40], negative LACO-OFDM (NLACO-OFDM) [41] and enhanced negative ADO-OFDM (eNADO-OFDM) [42] have also been proposed where they are combined with the corresponding HACO-OFDM, LACO-OFDM and eADO-OFDM, respectively. In these schemes, for intermediate illumination level the dimming target was achieved by adjusting the frames proportion of HACO-OFDM (LACO-OFDM, eADO-OFDM) to NHACO-OFDM (NLACO-OFDM, eNADO-OFDM), while for low and high illumination levels the scaling factors and DC bias were used to adjust the dimming level. However, these schemes do not achieve a continuous and arbitrary dimming level because of the proportion of the two kinds of signals not being a continuous value.

B. Contributions

A comprehensive overview including several typical O-OFDM schemes for VLC is listed in Table I in a comparison with our paper in terms of SE, EE, computation complexity (CC), time delay, dimming control function, optimization and dimming level, where N and T denote points number and time delay of a single inverse fast Fourier transform (IFFT) or FFT process, respectively. Besides, L is the maximum layer number of LACO-OFDM, and T_{PWM} represents the extra processing time delay for PWM signal in RPO-OFDM scheme. In Table I, the number of complex multiplications in a standard IFFT/FFT process equals to $N\log_2 N$ and the CC of complex additions is small enough to neglect compared with complex multiplications. For LACO-OFDM, the iterative receiver structure leads to the highest CC although still less than 5 times of ACO-OFDM, on the other hand, the demodulation delay climbs up constantly with the increment of loop times. However, the time delays at the transmitter are all the same because a parallel structure can be employed to send data at the same time [43]. For RPO-OFDM, it rarely supports a continuous dimming level (i.e. discrete) except for its biggest drawback of low SE, since the duty cycle is adjusted according to the reversed ACO-OFDM symbols. For example, in [37] there are 10 ACO-OFDM symbols in a PWM signal cycle so that the achievable duty cycle of RPO-OFDM has 11 values, i.e. 11 dimming levels. In addition, even though the signal unit of ACO-OFDM symbol can be further divided to transmit both on the "On" and "Off" stages when time-synchronization is perfect, the resolution of PWM signal also makes it be challenging to vary continuously, especially when extremely high frequency PWM signals are required for high rate O-OFDM VLC transmission.

In this paper, we extend the work in [14] to indoor VLC dimming scenarios and propose the novel dimmable THO-OFDM (DTH-OFDM) scheme, where dimming factors and DC bias can be jointly adjusted to satisfy the desirable dimming target form low illumination to high illumination intensities. By using convex optimization for bit error ratio (BER) and SE, the proposed DTH-OFDM achieves a continuous and arbitrary dimming range from low to high dimming levels with better performance as well as a lower CC and time delay, where the solved parameters in convex optimization algorithm can be calculated and stored in advance without extra CC and time delay at the receiver. More specifically, the main contributions of this paper are summarized as follows.

- A novel spectrum-efficient DTH-OFDM scheme having a simple triple-layer structure is proposed for indoor dimmable VLC. For the typical indoor line-of-sight (LOS) VLC channel, a dimming system model is introduced considering various practical scenarios from low illumination to high illumination intensities.
- By using the practical indoor VLC channel model, comprehensive performance analysis and simulation for DTH-OFDM including probability density function (PDF), BER, SE and EE are carried out, which are utilized to optimize and solve the joint dimming control and optimal power allocation problem.
- The optimal optical power allocation for THO-OFDM is investigated to achieve the minimum BER. The analytical BER expression for THO-OFDM is derived and we prove that, the average BER is a convex function with regards to two power allocation factors, therefore a global search algorithm can be adopted to solve the problem.
- The joint maximum SE and minimum BER problem is proposed, where we optimize the dimming and communications functions by considering formulating the jointed problem into three sub-problems based on the low, medium, and high dimming levels. Unlike the other existing schemes in the literature, our dimming adjustment relies on the dimming factor and DC bias rather than the proportion of two kinds of signals to achieve the continuous and arbitrary dimming target.

The rest of this paper is organized as follows. In Section II, THO-OFDM is presented, followed by the introduction of the

TABLE I
A COMPREHENSIVE LIST OF THE EXISTING TYPICAL PAPERS ON THE TOPIC OF O-OFDM VLC

	Year	SE	EE	CC		Delay		Dimming Control	Optimization	Dimming Level
				Tx	Rx	Tx	Rx			
DCO-OFDM [17]	1996	High	Low	$O(N\log_2 N)$	$O(N\log_2 N)$	$T\log_2 N$	$T\log_2 N$	×	×	×
ACO-OFDM [18]	2006	Low	High	$O(N\log_2 N)$	$O(N\log_2 N)$		$T\log_2 N$	×	×	×
HACO-OFDM [21]	2014	Medium	Medium	$O(2N\log_2 N)$	$O(3N\log_2 N)$		$3T\log_2 N$	×	×	×
LACO-OFDM [26]	2015	High	Medium	$O\left((2-1/2^{L-1})N\log_2 N\right)$	$O\left((5-1/2^{L-3})N\log_2 N\right)$		$(2L+1)T\log_2 N - L^2T + LT$	×	×	×
THO-OFDM [14]	2020	High	Medium	$O(N\log_2 N) + O(\frac{3N}{4}\log_2 \frac{N}{2})$	$O(2N\log_2 N) - N$		$3T\log_2 N - 2N$	×	×	×
RPO-OFDM [37]	2013	Low	Low	$O(N\log_2 N)$	$O(N\log_2 N)$		$T\log_2 N + T_{\mathrm{PWM}}$	✓	×	Discrete
AHO-OFDM [38]	2015	Medium	Low	$O(2N\log_2 N)$	$O(3N\log_2 N)$		$3T\log_2 N$	✓	×	Discrete
HLACO-OFDM [41]	2018	High	Low	$O\left((2-1/2^{L-1})N\log_2 N\right)$	$O\left((5-1/2^{L-3})N\log_2 N\right)$		$(2L+1)T\log_2 N - L^2T + LT$	✓	SE	Discrete
This work		High	Low	$O(N\log_2 N) + O(\frac{3N}{4}\log_2 \frac{N}{2})$	$O(2N\log_2 N) - N$		$3T\log_2 N - 2N$	✓	BER and SE	Continuous

proposed DTH-OFDM scheme for indoor VLC in Section III. In Section IV, theoretical analysis for PDF, BER, SE and EE of the DTH-OFDM system are given. Problem formulations for joint dimming control and optimal power allocation are presented in Section V, whereas in Section VI numerical results are used for evaluation of the system performance with dimming. Finally, conclusions are drawn in Section VII.

II. THO-OFDM SYSTEM

In IM/DD OFDM-based VLC systems, the OFDM signal must be both real and positive. Various single-layer optical-OFDM schemes such as DCO-OFDM, ACO-OFDM (U-OFDM), PAM-DMT have been proposed. Layered/enhanced optical-OFDM schemes of LACO-OFDM (eU-OFDM), ALACO-OFDM and ASE-DMT can further reduce the SE gap between ACO-OFDM and DCO-OFDM with high EE by means of infinite layers superimposition, but at the cost of increased hardware complexity, which is not desirable. THO-OFDM contains triple-layer signals of *N*-point ACO-OFDM, *N*/2-point ACO-OFDM, and *N*/2-point PAM-DMT [14].

In THO-OFDM, the first layer *N*-point QAM data in odd SCs can be represented as $X_{\mathrm{ACO}}^{(1)} = [0, X_1, 0, X_3, ..., X_{N/2-1}, 0, X_{N/2-1}^*, 0, ..., X_3^*, 0, X_1^*]$, where *N* is the number of SCs and the symbol $*$ denotes the conjugate symmetric operation. Following the IFFT process, the time-domain bipolar signal can be expressed as

$$x(n) = \frac{1}{\sqrt{N}} \sum_{k=0}^{N-1} X(k) \exp\left(-j\frac{2\pi}{N}kn\right), n = 0, 1, ..., N-1, \tag{1}$$

where the time-domain signal $x(n)$ has the antisymmetric property given as

$$x(n) = -x(n + N/2), n = 0, 1, ..., N/2 - 1. \tag{2}$$

Then, the unipolar ACO-OFDM signal for the first layer can be obtained by means of negative clipping without losing any useful information due to the antisymmetric property, which is given by

$$x_{\mathrm{THO}}^{(1)} = \begin{cases} x_n, x_n \geq 0, \\ 0, x_n < 0. \end{cases} \tag{3}$$

Note, the clipping noise of ACO-OFDM in the first layer falls on even SCs, therefore the even SCs can be used to carry data after removing the clipping noise. The second layer *N*/2-point QAM signal and the third layer *N*/2-point PAM signal are respectively defined as

$$X_{\mathrm{ACO}}^{(2)} = [0, X_1, 0, X_3, 0, ..., X_{N/4-1}, 0, X_{N/4-1}^*, ..., 0, X_3^*, 0, X_1^*], \tag{4}$$

$$X_{\mathrm{PAM}}^{(3)} = j[0, 0, P_2, 0, ..., P_{N/4-2}, 0, 0, 0, -P_{N/4-2}, ..., 0, -P_2, 0], \tag{5}$$

where $j = \sqrt{-1}$ and $P_k (k = 2, 4, ..., N/4 - 2)$ are PAM symbols. Following IFFT and negative clipping, the *N*/2-point unipolar signals of the second and third layers can be obtained, which corresponds to $x_{\mathrm{ACO}}^{(2)}$ and $x_{\mathrm{PAM}}^{(3)}$, respectively. To compensate for the length difference, a 2-time repeat operation is carried separately. Here, we denote the repeated *N*-point signals of the second and third layer as $x_{\mathrm{THO}}^{(2)} = [x_{\mathrm{ACO}}^{(2)}, x_{\mathrm{ACO}}^{(2)}]$ and $x_{\mathrm{THO}}^{(3)} = [x_{\mathrm{PAM}}^{(3)}, x_{\mathrm{PAM}}^{(3)}]$, respectively. It has been proved in the frequency domain that, $X_{\mathrm{THO}}^{(2)} = \mathcal{F}(x_{\mathrm{THO}}^{(2)})$ occupy the 2*k*-th$(k = 1, 3, ..., N/2 - 1)$ SCs and $X_{\mathrm{THO}}^{(3)} = \mathcal{F}(x_{\mathrm{THO}}^{(3)})$ occupy the 2*m*-th$(m = 2, 4, ..., N/2 - 2)$ SCs while the rest of SCs are zero [14], where the symbol $\mathcal{F}(\cdot)$ represents FFT. Therefore, $X_{\mathrm{THO}}^{(1)}$, $X_{\mathrm{THO}}^{(2)}$, and $X_{\mathrm{THO}}^{(3)}$ can be combined together using different SCs with no inter-carrier interference, which is expressed in the time-domain by

$$x_{\mathrm{THO}} = x_{\mathrm{THO}}^{(1)} + x_{\mathrm{THO}}^{(2)} + x_{\mathrm{THO}}^{(3)}. \tag{6}$$

III. DIMMING CONTROL BASED ON THO-OFDM VLC

In indoor applications, VLC offer the dual feature of illumination and data communications. In this section, we first introduce the channel model for the LOS VLC link followed by the system model for DTH-OFDM VLC.

A. Indoor VLC Channel Model

For practical VLC systems, the light should be adjusted intelligently to meet the requirements of human comfortableness and expectations. In general, the illumination of 300 lux (lumen per square meter) is suggested for office scenario and 500 lux for library and school scenarios. However, it is recommended to be 30 lux for personal computer task [31]. In special circumstances, the illumination intensity could be less or more, such as less than 10 lux for imperceptible VLC (in this case, VLC keeps communication function with low data rata while the illumination intensity is lower than the sensitivity threshold of human eyes) and more than 1000 lux for stadium, hospital and mall scenarios.

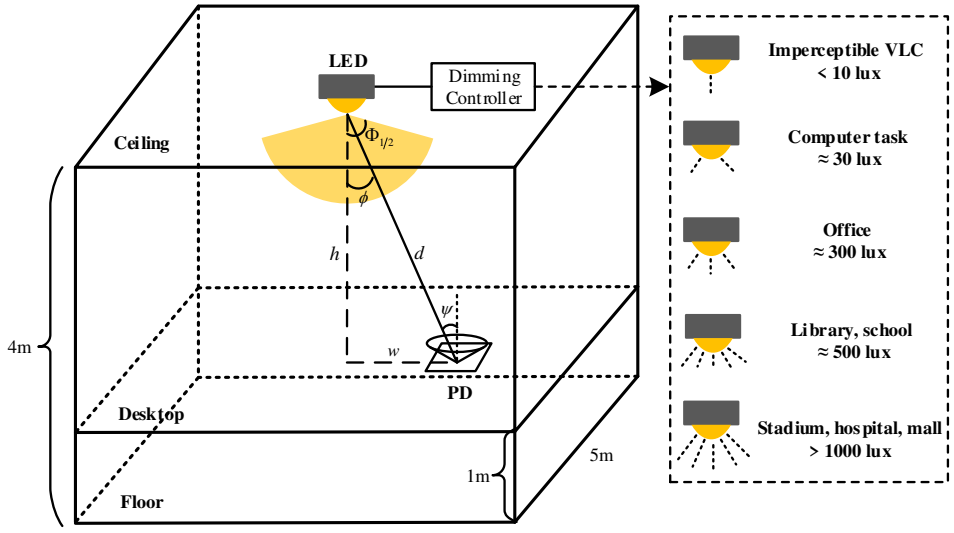

Fig. 1. Channel geometric model for indoor VLC systems.

Here, we consider an empty room with the dimensions of $5 \times 5 \times 4\text{m}^3$ (i.e., length, width, and height) as shown in Fig. 1, where a single LED and a photodetector (PD) are located on the centre point of ceiling and 1 m above the floor level, with the vertical, horizontal and direct distances of h, w and d respectively. The LED is intensity modulated with the information data. The power-current characteristic of LEDs normally displays some degree of nonlinearity, which will limit the maximum modulation index, i.e. signal to noise ratio (SNR). A number of mitigation schemes have been proposed to address the nonlinearity [43]. Thus the relationship between the forward current I and the forward voltage V (also between the power P and the I) can be quasi-linear over a limited range of $[V_L, V_H]$, where V_L and V_H denotes the turn-on and the maximum allowable voltages, respectively. Considering that the DC biased OFDM-VLC signal is a positive signal with DC bias being equal to V_L, the input voltage can be expressed as [45]

$$V_n = kx_n + V_L, \tag{7}$$

where $k = (V_H - V_L)/I_H$, I_H is the maximum I, and x_n is the transmitted signal of THO-OFDM.

For simplicity, we consider only the LOS path, with the DC gain modeled as a generalized Lambertian radiation pattern given as [45]

$$H_0 = \frac{(m+1)A}{2\pi d^2}\cos^m(\phi)T(\psi)g(\psi)\cos(\psi), \tag{8}$$

where Lambertian order $m = -1/\log 2(\cos(\Phi_{1/2}))$ and $\Phi_{1/2}$ is the LED semi-angle. A, ϕ and $T(\psi)$ denote the physical area of PD, light radiance angle and filter gain, respectively. $g(\psi)$ is the concentrator gain, which is defined as

$$g(\psi) = \begin{cases} \dfrac{n^2}{\sin^2\Psi_c}, & 0 \le \psi \le \Psi_c \\ 0, & \psi > \Psi_c \end{cases} \tag{9}$$

where Ψ_c and n are the field of view (FOV) and reflective index of the concentrator, respectively. The received signal at the receiver can be represented as [45]

$$r_n = H_0 R x_n + w_n, \tag{10}$$

where w_n denotes the additive white Gaussian noise (AWGN) and R denotes the comprehensive transform coefficient including the LED responsivity, *V-I* transfer and the PD responsivity.

B. System Model of DTH-OFDM

The schematic block diagram of the transmitter for the proposed DTH-OFDM system is illustrated in Fig. 2. The generated triple-layer unipolar optical-OFDM signals $x_{\text{THO}}^{(1)}$, $x_{\text{THO}}^{(2)}$ and $x_{\text{THO}}^{(3)}$ are scaled by the dimming factors α_i $(i = 1, 2, 3)$ prior to being DC biased I_{bias}, which is given as

$$x_{\text{DTH}} = \alpha_1 x_{\text{THO}}^{(1)} + \alpha_2 x_{\text{THO}}^{(2)} + \alpha_3 x_{\text{THO}}^{(3)} + I_{\text{bias}}. \tag{11}$$

Note that, α_i (can be either positive or negative) and I_{bias} are used for setting the dimming level. Based on the central limit theorem, the conventional ACO-OFDM and PAM-DMT have a clipped Gaussian distribution as given by [46]

$$f_{x_{\text{ACO}}}(w) = \frac{1}{\sqrt{2\pi}\sigma_{\text{ACO}}}\exp\left(\frac{-w^2}{2\sigma_{\text{ACO}}^2}\right)u(w) + \frac{1}{2}\delta(w), \tag{12}$$

$$f_{x_{\text{PAM}}}(w) = \frac{1}{\sqrt{2\pi}\sigma_{\text{PAM}}}\exp\left(\frac{-w^2}{2\sigma_{\text{PAM}}^2}\right)u(w) + \frac{1}{2}\delta(w), \tag{13}$$

where σ_{ACO} and σ_{PAM} are the root mean square (RMS) of the unclipped ACO-OFDM and PAM-DMT signals, respectively. $u(w)$ is the unit step function and $\delta(w)$ is the Dirac delta function. Then, the average optical power of ACO-OFDM and PAM-DMT are given, respectively as

$$E\left(x_{\text{ACO}}\right) = \int_0^\infty w f_{x_{\text{ACO}}}(w)dw = \frac{\sigma_{\text{ACO}}}{\sqrt{2\pi}}, \tag{14}$$

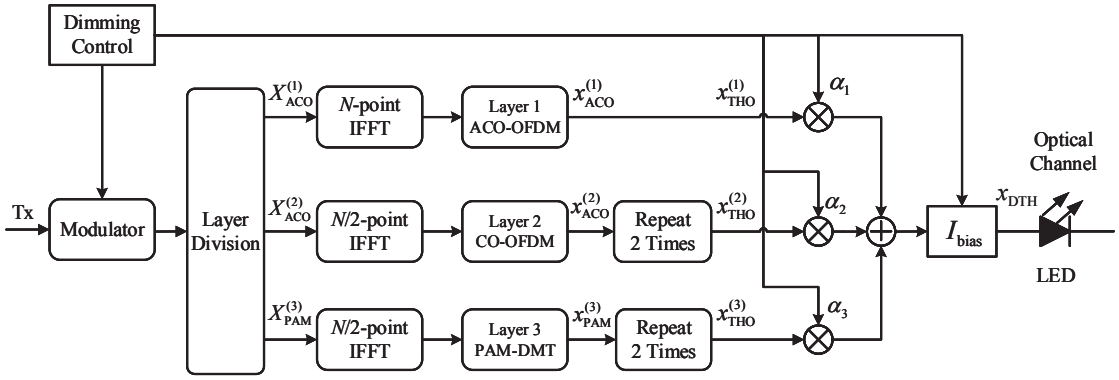

Fig. 2. Block diagram of transmitter for the proposed DTH-OFDM system.

$$E\left(x_{\mathrm{PAM}}\right)=\int_0^{\infty} w f_{x_{\mathrm{PAM}}}(w)dw=\frac{\sigma_{\mathrm{PAM}}}{\sqrt{2\pi}}. \tag{15}$$

Therefore, the average current amplitude of DTH-OFDM signal denoted as the expected value of x_{DTH} is given by

$$I_D=E\left(x_{\mathrm{DTH}}\right)=\alpha_1\frac{\sigma_1}{\sqrt{2\pi}}+\alpha_2\frac{\sigma_2}{\sqrt{2\pi}}+\alpha_3\frac{\sigma_3}{\sqrt{2\pi}}+I_{\mathrm{bias}}, \tag{16}$$

where the σ_i $(i=1,2,3)$ represents the RMS of the *i*-th layer signal in DTH-OFDM. Since the transfer characteristic of the LED is considered to be quasi-linear over a limited range of $[I_L, I_H]$, where I_L is the minimum drive current for the LED, the dimming level of the DTH-OFDM can be defined as

$$\eta=\frac{I_D-I_L}{I_H-I_L}, \tag{17}$$

where η is within the range of $[0,1]$.

IV. Performance analysis of DTH-OFDM

In this section, we carry out comprehensive performance analysis of the proposed DTH-OFDM system including PDF, BER, SE and EE.

A. PDF

From the perspective of signal distribution, we derive the PDF of DTH-OFDM for the optimal values of α_{i} and I_{bias}. Based on (11), the PDF of DTH-OFDM can be calculated by the convolution of the PDFs of triple-layer signals, given by [46]

$$f_{x_{\mathrm{DTH}}}(w)=f_{\alpha_1 x^{(1)}_{\mathrm{THO}}}(w)\otimes f_{\alpha_2 x^{(2)}_{\mathrm{THO}}}(w)\otimes f_{\alpha_3 x^{(3)}_{\mathrm{THO}}}(w), \tag{18}$$

where $\otimes$ represents the convolutional operation. Note I_{bias} is not considered here since it is a constant parameter. According to (12) and (13), the PDF of double-layer ACO-OFDM signals can be first derived as

$$\begin{aligned}&f_{\alpha_1 x^{(1)}_{\mathrm{THO}}}(w)\otimes f_{\alpha_2 x^{(2)}_{\mathrm{THO}}}(w)=\int_{-\infty}^{\infty} f_{\alpha_1 x^{(1)}_{\mathrm{THO}}}(l) f_{\alpha_2 x^{(2)}_{\mathrm{THO}}}(w-l)dl\\&=\int_{-\infty}^{\infty}\left[\frac{1}{\sqrt{2\pi}\alpha_1\sigma_1}\exp\left(\frac{-l^2}{2\alpha_1^2\sigma_1^2}\right)u[sgn(\alpha_1)l]+\frac{1}{2}\delta(l)\right]\times\\&\left[\frac{1}{\sqrt{2\pi}\alpha_2\sigma_2}\exp\left(\frac{-(w-l)^2}{2\alpha_2^2\sigma_2^2}\right)u[sgn(\alpha_2)(w-l)]+\frac{1}{2}\delta(w-l)\right]dl,\end{aligned} \tag{19}$$

where $\mathrm{sgn}(\cdot)$ represents symbolic function, which satisfies $\mathrm{sgn}(\cdot)=1$ if $(\cdot)>0$ and $\mathrm{sgn}(\cdot)=-1$ if $(\cdot)<0$. To simplify the derivation process here, α_1 and α_2 are set to positive in the following. Therefore, (19) can be simplified to (please see Appendix A)

$$\begin{aligned}&f_{\alpha_1 x^{(1)}_{\mathrm{THO}}}(w)\otimes f_{\alpha_2 x^{(2)}_{\mathrm{THO}}}(w)=\\&\frac{1}{\sqrt{2\pi(\alpha_1^2\sigma_1^2+\alpha_2^2\sigma_2^2)}}\exp\left(-\frac{w^2}{2(\alpha_1^2\sigma_1^2+\alpha_2^2\sigma_2^2)}\right)\times\\&\left[Q\left(-\frac{\alpha_1\sigma_1 w}{\alpha_2\sigma_2\sqrt{\alpha_1^2\sigma_1^2+\alpha_2^2\sigma_2^2}}\right)-Q\left(-\frac{\alpha_2\sigma_2 w}{\alpha_1\sigma_1\sqrt{\alpha_1^2\sigma_1^2+\alpha_2^2\sigma_2^2}}\right)\right]\\&+\frac{1}{2\sqrt{2\pi}}\left[\frac{1}{\alpha_1\sigma_1}\exp(\frac{-w^2}{2\alpha_1^2\sigma_1^2})+\frac{1}{\alpha_2\sigma_2}\exp(\frac{-w^2}{2\alpha_2^2\sigma_2^2})\right]u(w)\\&+\frac{1}{4}\delta(w),\end{aligned} \tag{20}$$

where function $Q(\cdot)$ is the tail probability of the standard normal distribution given by $Q\left(\xi\right)=\frac{1}{\sqrt{2\pi}}\int_{\xi}^{\infty}\exp(-\frac{u^2}{2})du$.

Similarly, we can derive the PDF of the DTH-OFDM with triple-layer according to (18)-(20), which is shown in Appendix A.

Since the amplitude of the DTH-OFDM signal is constrained by the dynamic range of LED, x_{THO} needs to be constrained within the range of $[I_L, I_H]$, which maybe result in undesirable clipping distortion. To estimate the undesirable clipping distortion, we introduce a scaling factor, which is given for the *i*-th layer signal as

$$\gamma_i=\frac{\frac{1}{2}\left[\mathrm{sgn}(\alpha_i)+1\right]I_H-\mathrm{sgn}(\alpha_i)I_{\mathrm{bias}}+\frac{1}{2}\left[\mathrm{sgn}(\alpha_i)-1\right]I_L}{|\alpha_i|\sigma_i}. \tag{21}$$

Therefore, the clipping probability is given as

$$P(x_{\mathrm{DTH}}>I_H)=P(\sum_{i=1}^{3}\alpha_i x^{(i)}_{\mathrm{THO}}>I_H-I_{\mathrm{bias}})=\int_{I_H-I_{\mathrm{bias}}}^{+\infty} f_{x_{\mathrm{DTH}}}(w)dw, \tag{22}$$

$$P(x_{\mathrm{DTH}}<I_L)=P(\sum_{i=1}^{3}\alpha_i x^{(i)}_{\mathrm{THO}}<I_L-I_{\mathrm{bias}})=\int_{-\infty}^{I_L-I_{\mathrm{bias}}} f_{x_{\mathrm{DTH}}}(w)dw. \tag{23}$$

Based on (18)-(23), the clipping probability is related to σ_i, (i.e. γ_i) and α_i, see Appendix A. For γ_i being lager, the

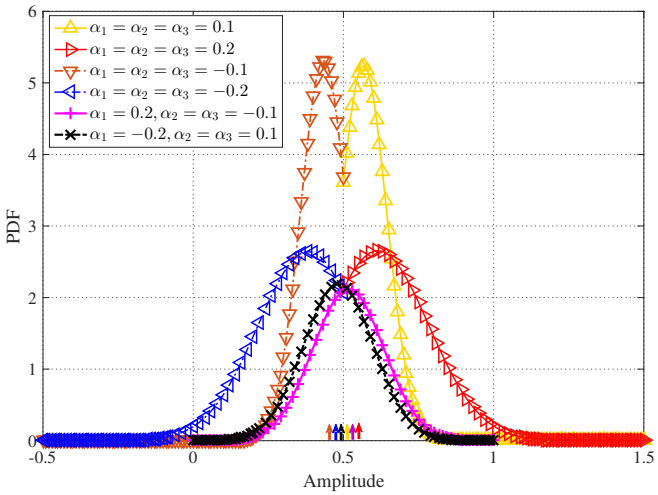

Fig. 3. PDFs of DTH-OFDM with various dimming factors α_i when $I_{\text{bias}}=0.5$, where six different colours arrows all represent the Dirac delta function in the point of I_{bias}.

probability of clipped signal is small. The simulated PDFs of the DTH-OFDM with various dimming factors of α_i are demonstrated in Fig. 3, which shows the PDF as a function of the normalized current amplitude for a range of α_i when $I_{\text{bias}}=0.5$ and $[I_L, I_H]=[0,1]$. Note, at I_{bias} of 0.5 the probability of amplitude is 0.125, which is equal to the integral value of $\frac{1}{8}\delta(\cdot)$. When values of DC bias below and above the optimum I_{bias} (i.e., 0.5), the PDF plots move to the left and right, respectively. This would increase the probability of clipping due to the LED nonlinearity, which is not desirable and needs to be avoided. Thus, the trade-off between dimming control and power allocation needs to be solved for achieving the optimal system performance, which is considered in the following sections.

B. BER Performance

Given that signals from different layers in DTH-OFDM are combined to make the time-domain signal, an essential problem is the optimal power allocation amongst the layers to ensure optimal performance. Besides, the dimming function has an adverse effect on communication quality. This part derives the average BER of THO-OFDM scheme from the conventional QAM and PAM formulas, which is necessary for helping us to solve the optimal power allocation and dimming control problems.

For conventional ACO-OFDM and PAM-DMT with constellation sizes of M_1 and M_2 respectively, the bit error probabilities can be formulated as [46], [47]

$$P_{b,\text{QAM}} \approx \frac{4\left(\sqrt{M_1}-1\right)}{\sqrt{M_1}\log_2 M_1} Q\left(\sqrt{\frac{3}{M_1-1}\frac{E_s}{N_0}}\right), \tag{24}$$

$$P_{b,\text{PAM}} \approx \frac{2\left(M_2-1\right)}{M_2\log_2 M_2} Q\left(\sqrt{\frac{6}{M_2^2-1}\frac{E_s}{N_0}}\right), \tag{25}$$

where E_s denotes the electrical energy per SC and N_0 represents noise power spectral density. Therefore, for the l-th$(l=1,2,3)$ layer the bit error probability can be derived as

$$\begin{aligned} P_{b,l} &= P_{b,1\sim l-1}P_{b,l|\overline{1\sim l-1}} + (1-P_{b,1\sim l-1})P_{b,l|1\sim l-1} \\ &= P_{b,l|1\sim l-1} + P_{b,1\sim l-1}(P_{b,l|\overline{1\sim l-1}} - P_{b,l|1\sim l-1}), \end{aligned} \tag{26}$$

where $P_{b,l|1\sim l-1}$ and $P_{b,l|\overline{1\sim l-1}}$ denote the conditional probability of errors considering that, the signals from the first layer to the $(l-1)$-th layers are demodulated correctly and incorrectly, respectively. Note, for high SNR, the second term in (26) is smaller than the first term and therefore can be neglected, thus the estimated bit error probability is given as

$$P_{b,l} \approx P_{b,l|1\sim l-1} \approx \begin{cases} \frac{4\left(\sqrt{M_1}-1\right)}{\sqrt{M_1}\log_2 M_1} Q\left(\sqrt{\frac{3E_{s,l}}{(M_1-1)N_0}}\right), l=1,2 \\ \frac{2\left(M_2-1\right)}{M_2\log_2 M_2} Q\left(\sqrt{\frac{6E_{s,l}}{(M_2^2-1)N_0}}\right), l=3 \end{cases} \tag{27}$$

where M_1 is the constellation size for the layers 1 and 2 for simplicity, M_2 is the constellation size for layer 3 and $E_{s,l}$ denotes the electrical energy per SC at the l-th layer of THO-OFDM. Therefore, the average bit error probability of THO-OFDM can be derived as [14]

$$\begin{aligned} P_{b,\text{THO}} &= \frac{\frac{N}{4}\log_2 M_1 \cdot P_{b,1} + \frac{N}{8}\log_2 M_1 \cdot P_{b,2} + \left(\frac{N}{8}-1\right)\log_2 M_2 \cdot P_{b,3}}{\frac{N}{4}\log_2 M_1 + \frac{N}{8}\log_2 M_1 + \left(\frac{N}{8}-1\right)\log_2 M_2} \\ &\approx \frac{N\left(\sqrt{M_1}-1\right)}{\lambda\sqrt{M_1}} Q\left(\sqrt{\frac{3E_{s,1}}{(M_1-1)N_0}}\right) + \frac{N\left(\sqrt{M_1}-1\right)}{2\lambda\sqrt{M_1}} \times \\ &\quad Q\left(\sqrt{\frac{3E_{s,2}}{(M_1-1)N_0}}\right) + \frac{(N-8)(M_2-1)}{4\lambda M_2} Q\left(\sqrt{\frac{6E_{s,3}}{(M_2^2-1)N_0}}\right), \end{aligned} \tag{28}$$

where $\lambda = \frac{N}{4}\log_2 M_1 + \frac{N}{8}\log_2 M_1 + \left(\frac{N}{8}-1\right)\log_2 M_2$.

C. SE and EE

In this part, we investigate the relationship between SE and EE of DTH-OFDM for indoor VLC, which are defined respectively as [45]

$$\eta_{\text{SE}} = \frac{C}{W}, \tag{29}$$

$$\eta_{\text{EE}} = \frac{C}{P}. \tag{30}$$

where C is the link capacity, W is the entire bandwidth, and P is the sum power cost. Note, we only consider the power consumption by the LED for simplicity. For conventional ACO-OFDM with clipped amplitude by half in the frequency-domain, and PAM-DMT, the SNRs for each SC are given as, respectively [45]

$$\xi_{\text{ACO}} = \frac{\frac{1}{4}H_0^2R^2\sigma_{\text{A}}^2}{\sigma_n^2} = \frac{H_0^2R^2\sigma_{\text{A}}^2}{4\sigma_n^2}, \tag{31}$$

$$\xi_{\text{PAM}} = \frac{\frac{1}{4}H_0^2R^2\sigma_{\text{P}}^2}{\frac{1}{2}\sigma_n^2} = \frac{H_0^2R^2\sigma_{\text{P}}^2}{2\sigma_n^2}, \tag{32}$$

where σ_{A}^2 denotes the variance of the modulated complex-valued symbols $X_{2k+1}(k=0,1,...,N/4-1)$, $\sigma_n^2=N_0W/N$ is the noise power and σ_{P}^2 denotes the variance of the modulated PAM symbols.

In THO-OFDM system, the variance of the modulated triple-layer complex-valued symbols is assumed to be normalized as σ^2. Thus, for the indoor DTH-OFDM VLC link the total capacity C_{DTH} and the sum power cost P_{DTH} for LED are given as, respectively

$$\begin{aligned} C_{\mathrm{DTH}} &= \frac{W}{4}\log_2(1+\xi_{\mathrm{ACO},1}) + \frac{W}{8}\log_2(1+\xi_{\mathrm{ACO},2}) + \\ &\quad \frac{(N-8)W}{16N}\log_2(1+\xi_{\mathrm{PAM},3}) \\ &= \frac{W}{4}\log_2\left(1+\frac{H_0^2R^2\alpha_1^2\sigma^2}{4\sigma_n^2}\right) + \frac{W}{8}\log_2\left(1+\frac{H_0^2R^2\alpha_2^2\sigma^2}{4\sigma_n^2}\right) \\ &\quad + \frac{(N-8)W}{16N}\log_2\left(1+\frac{H_0^2R^2\alpha_3^2\sigma^2}{2\sigma_n^2}\right). \end{aligned} \tag{33}$$

$$\begin{aligned} P_{\mathrm{DTH}} &= E\left[U_n I_n\right] = E\left[(kx_{\mathrm{DTH}} + U_{\mathrm{L}})x_{\mathrm{DTH}}\right] \\ &= kE\left[x_{\mathrm{DTH}}^2\right] + U_{\mathrm{L}}E\left[x_{\mathrm{DTH}}\right]. \end{aligned} \tag{34}$$

Note, the optimal power allocation coefficients for DTH-OFDM have not been taken into account here and will be addressed in the next section. Since triple-layer signals occupy *N*/2-, *N*/4- and (*N*/4−2)-point SCs respectively and the remaining SCs are set to zeros in the frequency-domain, then using Parseval's theorem the relationship between σ_i^2 and σ^2 is given by

$$\sigma_i^2 = \begin{cases} \dfrac{\sigma^2}{2^i}, i = 1, 2 \\ \dfrac{(N-8)\sigma^2}{4N}, i = 3 \end{cases} \tag{35}$$

By substituting (35) into (16), we have the expected value of x_{DTH} as

$$\begin{aligned} E[x_{\mathrm{DTH}}] &= \frac{\alpha_1\sigma_1}{\sqrt{2\pi}} + \frac{\alpha_2\sigma_2}{\sqrt{2\pi}} + \frac{\alpha_3\sigma_3}{\sqrt{2\pi}} + I_{\mathrm{bias}} \\ &= \frac{\alpha_1\sigma}{2\sqrt{\pi}} + \frac{\alpha_2\sigma}{2\sqrt{2\pi}} + \frac{\alpha_3\sigma}{\sqrt{2\pi}}\sqrt{\frac{(N-8)}{4N}} + I_{\mathrm{bias}}. \end{aligned} \tag{36}$$

Note, for large N, for example 512, we have

$$E[x_{\mathrm{DTH}}] \approx \frac{\alpha_1\sigma}{2\sqrt{\pi}} + \frac{\alpha_2\sigma}{2\sqrt{2\pi}} + \frac{\alpha_3\sigma}{2\sqrt{2\pi}} + I_{\mathrm{bias}}. \tag{37}$$

The mean square value of x_{DTH}^2 can be derived as

$$\begin{aligned} E[x_{\mathrm{DTH}}^2] &= \sum_{l=1}^{3}\alpha_i^2 E[(x_{\mathrm{DTH}}^{(l)})^2] + 2I_{\mathrm{bias}}\sum_{l=1}^{3}\alpha_l E[x_{\mathrm{DTH}}^{(l)}] \\ &+ 2\sum_{i=1}^{2}\sum_{j=i+1}^{3}\alpha_i\alpha_j E[x_{\mathrm{DTH}}^{(i)}x_{\mathrm{DTH}}^{(j)}] + I_{\mathrm{bias}}^2 \\ &\approx \frac{\sigma^2}{8}(2\alpha_1^2+\alpha_2^2+\alpha_3^2) + I_{\mathrm{bias}}(\frac{\alpha_1\sigma}{\sqrt{\pi}} + \frac{\alpha_2\sigma}{\sqrt{2\pi}} + \frac{\alpha_3\sigma}{\sqrt{2\pi}}) \\ &+ 2\alpha_i\alpha_j\sum_{i=1}^{2}\sum_{j=i+1}^{3}E[x_{\mathrm{DTH}}^{(i)}x_{\mathrm{DTH}}^{(j)}] + I_{\mathrm{bias}}^2 \\ &\triangleq \frac{\sigma^2}{8}(2\alpha_1^2+\alpha_2^2+\alpha_3^2) + I_{\mathrm{bias}}(\frac{\alpha_1\sigma}{\sqrt{\pi}} + \frac{\alpha_2\sigma}{\sqrt{2\pi}} + \frac{\alpha_3\sigma}{\sqrt{2\pi}}) \\ &+ \sigma^2(\frac{\alpha_1\alpha_2}{2\sqrt{2\pi}} + \frac{\alpha_1\alpha_3}{2\sqrt{2\pi}} + \frac{\alpha_2\alpha_3}{4\pi}) + I_{\mathrm{bias}}^2, \end{aligned} \tag{38}$$

where step "$\approx$" is also derived based on when the N is large while step "$\triangleq$" is derived based on the different layers of DTH-OFDM, which are subject to independent distribution, i.e., $E[x_{\mathrm{DTH}}^{(i)}x_{\mathrm{DTH}}^{(j)}] = E[x_{\mathrm{DTH}}^{(i)}]E[x_{\mathrm{DTH}}^{(j)}]$. Here, the SE for indoor DTH-OFDM VLC is given as

$$\begin{aligned} \eta_{\mathrm{SE}} &= \frac{C_{\mathrm{DTH}}}{W} \\ &= \frac{1}{4}\log_2\left(1+\frac{H_0^2R^2\alpha_1^2\sigma^2}{4\sigma_n^2}\right) + \frac{1}{8}\log_2\left(1+\frac{H_0^2R^2\alpha_2^2\sigma^2}{4\sigma_n^2}\right) \\ &+ \frac{(N-8)}{16N}\log_2\left(1+\frac{H_0^2R^2\alpha_3^2\sigma^2}{2\sigma_n^2}\right), \end{aligned} \tag{39}$$

and the EE can be given as (40) on the top of next page. Therefore, the relationship between SE and EE can be formulated as

$$\eta_{\mathrm{EE}} = \frac{W\eta_{\mathrm{SE}}}{U_{\mathrm{L}}\sigma(\frac{\alpha_1}{2\sqrt{\pi}}+\frac{\alpha_2}{2\sqrt{2\pi}}+\frac{\alpha_3}{2\sqrt{2\pi}})+U_{\mathrm{L}}I_{\mathrm{bias}}+kE\left[x_{\mathrm{DTH}}^2\right]}. \tag{41}$$

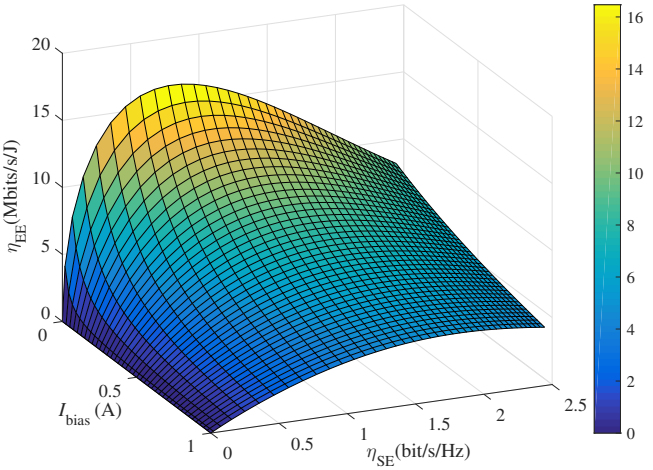

Fig. 4. I_{bias} and η_{SE} versus η_{EE} of DTH-OFDM in indoor VLC.

Using (41) and the simulation parameters given in Table II, we have plotted the EE as the function of I_{bias} and SE for DTH-OFDM VLC with the dimming factors set as $\alpha_i = 1$, see Fig. 4. Note, the optimal power allocation is not considered here for simplicity. As observed in Fig. 4, the EE is a concave function of SE for a given I_{bias} and it is also a monotone decreasing function of I_{bias} for a given SE.

V. Joint Dimming Control and Optimal Power Allocation

In this section, we explore the joint dimming control and the optimal power allocation strategy for indoor DTH-OFDM VLC. First, using convex optimization we derive the optimal power allocation coefficients between triple-layer branches to achieve the minimum BER. This is followed by problem formulation for the dimming control where we consider three dimming stages to achieve the dynamic lightness adjustment.

$$\eta_{\mathrm{EE}}=\frac{C_{\mathrm{THO}}}{P}=\frac{\frac{W}{4}\log_2\left(1+\frac{H_0^2R^2\alpha_1^2\sigma^2}{4\sigma_n^2}\right)+\frac{W}{8}\log_2\left(1+\frac{H_0^2R^2\alpha_2^2\sigma^2}{4\sigma_n^2}\right)+\frac{(N-8)W}{16N}\log_2\left(\frac{1+H_0^2R^2\alpha_3^2\sigma^2}{2\sigma_n^2}\right)}{U_{\mathrm{L}}\sigma(\frac{\alpha_1}{2\sqrt{\pi}}+\frac{\alpha_2}{2\sqrt{2\pi}}+\frac{\alpha_3}{2\sqrt{2\pi}})+U_{\mathrm{L}}I_{\mathrm{bias}}+kE\left[x_{\mathrm{THO}}^2\right]}. \tag{40}$$

TABLE II
SIMULATION PARAMETERS OF FIG. 4 AND FIG. 9

Parameter	Value
Bandwidth, W	20 MHz
QAM modulation order, M_1	16
PAM modulation order, M_2	4
Vertical distance, h	3 m
Horizontal distance, w	0 m
LED semiangle, $\Phi_{1/2}$	60°
Receiver FOV semiangle, Ψ_c	80°
Reflective index, n	1.5
Detector area, A	0.0001 m^2
Maximum voltage, V_H	3.4 V
Turn-on voltage, V_L	2.7 V
Maximum current, I_H	1 A
Transfer coefficient, R	0.5
Subcarriers number, N	512
Optical filter gain, $T(\psi)$	1
Noise power spectral density, N_0	10E-18 A^2/Hz

A. Optimal Power Allocation - Minimize BER

For THO-OFDM, we define the proportion of optical power allocated to layer 1 and layer 2 are β_1 and β_2, respectively that are given by

$$\beta_1=\frac{P_{o,1}}{P_{o,1}+P_{o,2}+P_{o,3}}\quad\text{and}\quad\beta_2=\frac{P_{o,2}}{P_{o,1}+P_{o,2}+P_{o,3}}, \tag{42}$$

where $0<\beta_1<1$ and $0<\beta_2<1$. Substituting (42) into (28), we have

$$P_{b,\mathrm{THO}}\approx\frac{N\left(\sqrt{M_1}-1\right)}{\lambda\sqrt{M_1}}Q\left(\sqrt{\frac{3\pi{\beta_1}^2}{(M_1-1)N_0}}\right)+\frac{N\left(\sqrt{M_1}-1\right)}{2\lambda\sqrt{M_1}}\times Q\left(\sqrt{\frac{3\pi{\beta_2}^2}{(M_1-1)N_0}}\right)+\frac{(N-8)\left(M_2-1\right)}{4\lambda M_2}Q\left(\sqrt{\frac{6\pi(1-\beta_1-\beta_2)^2}{(M_2^2-1)N_0}}\right), \tag{43}$$

where $E_{s,l}=\pi P_{o,l}^2$ [48] and $P_{o,1}+P_{o,2}+P_{o,3}$ are set to unity for simplicity of the following calculation. Since $Q(\cdot)$ is a continuous function in a bounded closed interval $[0,1]$ for both β_1 and β_2, $P_{b,\mathrm{THO}}$ is also a continuous function within its definitional domain. Furthermore, as proved in Appendix B, $P_{b,\mathrm{THO}}$ is a convex function. The extreme values of the double-variable function $P_{b,\mathrm{THO}}$ will only occur at points, where its gradient equals zero. Therefore, the optimum point (β_1,β_2) can be found by solving

$$\mathrm{diag}\left\{\nabla P_{b,\mathrm{THO}}(\beta_1,\beta_2)\right\}=0. \tag{44}$$

Here, symbol ∇ is Hamilton operator. The derivatives of $P_{b,\mathrm{THO}}$ are $\frac{\partial P_{b,\mathrm{THO}}}{\partial\beta_1}$ and $\frac{\partial P_{b,\mathrm{THO}}}{\partial\beta_2}$, therefore for solving (44) a nested algorithm using gradient descent is required. For a double-variable searching algorithm, however, its computation complexity and iteration times are much higher than single-variable. Inspiring by designing a low-complexity solving solution, we can simplify (44) using Theorem 1 to

$$\mathrm{diag}\left\{\nabla P_{b,\mathrm{THO}}(\beta_1,\beta_2)\right\}=0,\quad\text{s.t.}\quad\beta_1=\sqrt{2}\beta_2. \tag{45}$$

Theorem 1: For L-layer LACO-OFDM under the AWGN channel, define the proportion of optical power allocated to layer l ($1\le l\le L$) is β_l. To achieving the minimum average BER, the optimal optical power allocation solution for LACO-OFDM can be expressed as

$$\beta_{l-1}=\sqrt{2}\beta_l. \tag{46}$$

Proof: For LACO-OFDM, the electrical power of each SC in layer l is $E_{s,l}$, which should be equally distributed to achieve the minimum average BER [49], i,e, $E_{s,1}=E_{s,2}=\cdots=E_{s,l}$. Since only $N/2^l$ SCs are occupied in the l-th layer, i,e, $\sigma_l^2=E_{s,l}/2^l$ based on the Parseval's theorem, the relationship between the RMSs of unclipped layers can be expressed as [49]

$$\sigma_{l-1}=\sqrt{2}\sigma_l, \tag{47}$$

where $\sigma_l=\sqrt{2\pi}P_{o,l}$. Based on Theorem 1, we have $P_{o,l}=\beta_l\sum_{i=1}^{L}P_{o,i}$. Hence, the relationship between β_l can be derived, see Theorem 1. ■

Then, (45) can be written as

$$\left.\frac{\partial P_{b,\mathrm{THO}}}{\partial\beta_2}\right|_{\beta_1=\sqrt{2}\beta_2}=0. \tag{48}$$

Note, for high SNR, N_0 is small enough and can be ignored, therefore (48) can be approximately derived in terms of β_2 and (M_1,M_2) as given

$$3(M_2^2-1)\beta_2^2=2(M_1-1)(1-\sqrt{2}\beta_2-\beta_2)^2. \tag{49}$$

For $M_1=16$ and $M_2=4$, the optimal power allocation solution for THO-OFDM should satisfy $\beta_1=\sqrt{2}\beta_2\approx0.3886$. Besides, more cases between modulation order and optimal power allocation coefficients are listed in Table III. It is worth noting that 64QAM-8PAM has the same coefficients of β_l and β_2 compared with 16QAM-4PAM, which is because in this case modulation order satisfies $M_1=M_2^2$. Therefore, (49) has the same solutions.

TABLE III
OPTIMAL POWER ALLOCATION COEFFICIENTS FOR THO-OFDM UNDER VARIOUS MODULATION ORDERS M_1 and M_2

	4-4	16-4	16-8	64-8	64-16
β_1	0.2745	0.3886	0.2872	0.3886	0.2899
β_2	0.1941	0.2748	0.2031	0.2748	0.2050

A clear 3D version of the BER plot as the function of β_1 and β_2 with the contour map of a projection for 16-QAM and 4-PAM THO-OFDM under diffenent $\frac{E_b}{N_0}$ is provided in Fig. 5. Observe that, the BER always decreases in Fig. 5(a)-(d),

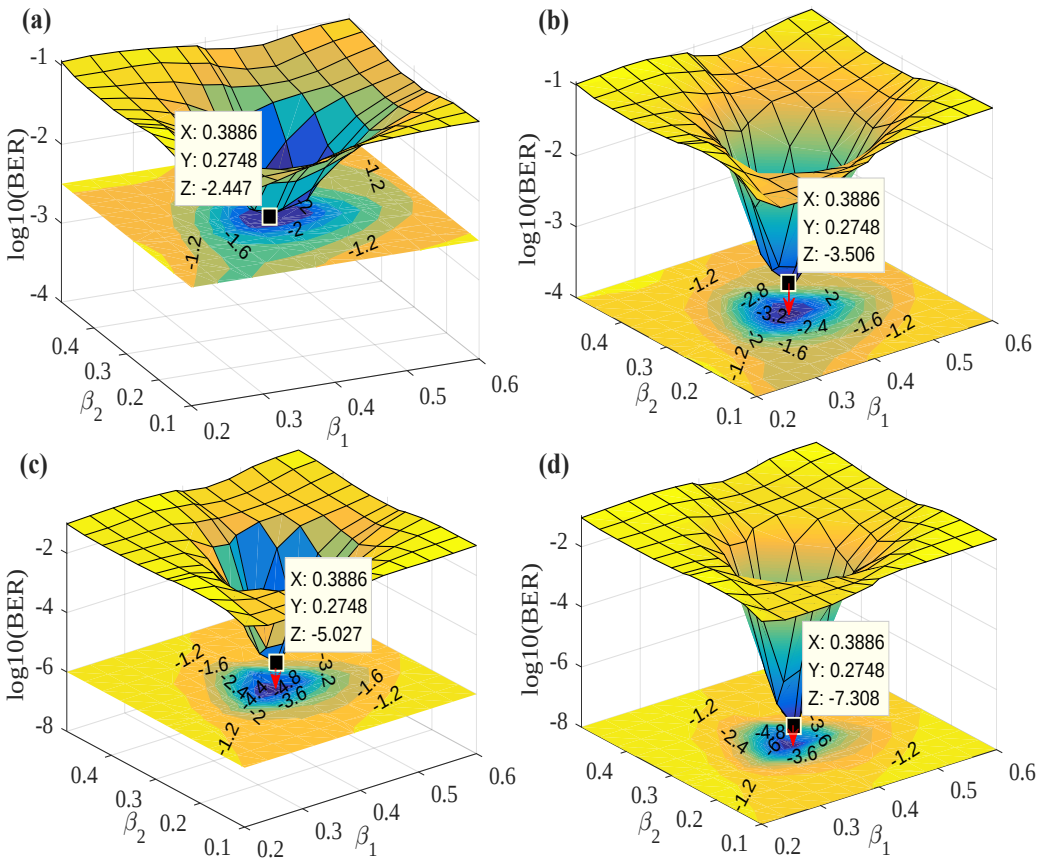

Fig. 5. BER performance of THO-OFDM and its contour map of the projection in X-O-Y plane v.s. β_1 and β_2 when using 16QAM and 4PAM, (a) $\frac{E_b}{N_0} = 14$ dB, (b) $\frac{E_b}{N_0} = 16$ dB, (c) $\frac{E_b}{N_0} = 18$ dB and (d) $\frac{E_b}{N_0} = 20$ dB.

reaching the minimum level at (β_1, β_2) = (0.3886, 0.2748), i.e., a global minimum point, which is consistent with the predicted result using (49). Besides, the minimum BER value decreases from $10^{-2.447}$ to $10^{-7.308}$ when $\frac{E_b}{N_0}$ increases from 14 dB to 20 dB.

B. Problem Formulation

In a typical VLC system, the key challenge is to achieve a continuous and wide dimming range while maintaining high quality data communications. We adjust α_i and I_{bias} to address this problem and achieve adjustable dynamic illumination by considering the minimum average BER, i.e., $P_{b,\text{THO}}$, and the maximum SE, i.e., η_{SE}. We consider the dimming range of η can be divided into three sections for different scenarios: (i) dimming stage I with $0 < \eta < \eta_L$; (ii) dimming stage II with $\eta_L \leq \eta \leq \eta_H$; and (iii) dimming stage III with $\eta_H < \eta < 1$, where η_L and η_{H} denote the low illumination and high illumination threshold levels, respectively.

1) Dimming Stage I ($0 < \eta < \eta_L$): For this, there is no need to introduce an extra bias level since α_i can be set be positive to dynamically adjust the dimming level. Thus, the constrained joint dimming control and optimal power allocation problem can be formulated as

$$
\begin{aligned}
(\text{P1}): \quad & \min_{\beta_1,\beta_2} \quad P_{b,\text{THO}} \\
& \text{s.t.} \quad \alpha_i > 0, \quad i = 1, 2, 3, && \text{(50a)} \\
& \qquad 0 < \beta_1, \beta_2 < 1, && \text{(50b)} \\
& \qquad I_{\text{bias}} = I_L, && \text{(50c)} \\
& \qquad \gamma_i \geq 4. && \text{(50d)}
\end{aligned}
$$

The objective function of problem (P1) is a convex function, which can be solved by the former subsection. Considering that, for DTH-OFDM the proportion of optical power allocated to the layers 1 and 2 are β_1 and β_2, i.e., $\beta_1 : \beta_2 : (1 - \beta_1 - \beta_2) = 1 : \frac{\beta_2}{\beta_1} : (\frac{1}{\beta_1} - 1 - \frac{\beta_2}{\beta_1})$, then (17) can be written as

$$
\eta = \frac{I_D - I_L}{I_H - I_L} \approx \frac{\alpha_1 \sigma}{2\sqrt{\pi}} + \frac{\alpha_2 \sigma}{2\sqrt{2\pi}} \frac{\beta_2}{\beta_1} + \frac{\alpha_3 \sigma}{2\sqrt{2\pi}} (\frac{1}{\beta_1} - 1 - \frac{\beta_2}{\beta_1}), \tag{51}
$$

where I_L and I_H are respectively set to 0 and 1 for simplicity, similarly for the stage II and III in the following parts. For the constraint (50d), i.e., C_{50d}, γ_i is defined as scaling factors to reduce undesirable clipping distortion due to the nonlinearity

of LED. Using (21) (35) and C_{50c}, C_{50d} can be formulated as

$$\gamma_i = \begin{cases} \dfrac{1}{\alpha_1\sigma_1} = \dfrac{\sqrt{2}}{\alpha_1\sigma} \geq 4, i = 1 \\ \dfrac{\beta_1}{\alpha_2\beta_2\sigma_2} = \dfrac{2\beta_1}{\alpha_2\beta_2\sigma} \geq 4, i = 2 \\ \dfrac{1}{\alpha_3(\frac{1}{\beta_1} - 1 - \frac{\beta_2}{\beta_1})\sigma_3} \approx \dfrac{2}{\alpha_3(\frac{1}{\beta_1} - 1 - \frac{\beta_2}{\beta_1})\sigma} \geq 4, i = 3 \end{cases} \tag{52}$$

Under the optimal power allocation solution, α_i should be set be the same for solve (P1), i.e., $\alpha_1 = \alpha_2 = \alpha_3 = \alpha$. Thus, (52) can be used to determine the adjustable range of α, then we have

$$0 < \alpha \leq \min\{\frac{\sqrt{2}}{4}, \frac{\beta_1}{2\beta_2}, \frac{\beta_1}{2(1-\beta_1-\beta_2)}\}, \tag{53}$$

where σ^2 is normalized to unity, β_1 and β_2 should satisfy $\beta_1 = \sqrt{2}\beta_2$ and the relationship in (49) under the objective function in (P1). Therefore, the dimming level can be dynamically adjust by α within the interval of $(0, \eta_L)$, which can be expressed as

$$\alpha = \frac{2\sqrt{2\pi}\eta}{\sqrt{2} - 1 + \frac{1}{\beta_1}}, \tag{54}$$

And η_L can be calculated by substituting $\alpha_{\max}$ into (54), which can be expressed as

$$\eta_L = \frac{(\sqrt{2} - 1 + \frac{1}{\beta_1})\alpha_{\max}}{2\sqrt{2\pi}}. \tag{55}$$

2) Dimming Stage II ($\eta_L \leq \eta \leq \eta_H$): In this case the dimming adjustment using α_i cannot be done considering the constraint C_{50d}. Therefore, dimming adjustment is achieved by using I_{bias}, where the objective functions are to achieve maximum η_{SE} and minimum $P_{b,\mathrm{THO}}$, as formulated below

$$\begin{aligned} (\mathrm{P2.1}): \quad & \max_{\alpha_i} \quad \eta_{\mathrm{SE}} \\ & \min_{\beta_1,\beta_2} \quad P_{b,\mathrm{THO}} \\ & \text{s.t.} \quad \alpha_i \neq 0, \ \ i = 1,2,3, && \text{(56a)} \\ & \qquad 0 < \beta_1, \beta_2 < 1, && \text{(56b)} \\ & \qquad I_{\mathrm{bias}} = \eta, && \text{(56c)} \\ & \qquad \gamma_i \geq 4. && \text{(56d)} \end{aligned}$$

Note that, the independent variables of two objective functions are independent of each other, although (P2.1) is a multi-objective programming problem. In the previous part, minimum $P_{b,\mathrm{THO}}$ problem has been given as (44) and then solved by convex optimization. Therefore, we can transform one solved objective function (44) into restriction, which can be formulated as

$$\begin{aligned} (\mathrm{P2.2}): \max_{\alpha_i} \quad & \eta_{\mathrm{SE}} \\ \text{s.t.} \quad & \alpha_i \neq 0, \ \ i = 1,2,3, && \text{(57a)} \\ & \mathrm{diag}\{\nabla P_{b,\mathrm{THO}}(\beta_1,\beta_2)\} = 0, && \text{(57b)} \\ & \sqrt{2}\alpha_1 + \frac{\beta_2}{\beta_1}\alpha_2 + \left(\frac{1}{\beta_1} - 1 - \frac{\beta_2}{\beta_1}\right)\alpha_3 = 0, && \text{(57c)} \\ & \gamma_i \geq 4. && \text{(57d)} \end{aligned}$$

Algorithm 1: Global search algorithm for solving (P2.2)

Input: target illumination level η, loop times n, M_1, M_2, H_0, R, σ_n^2, N
Output: α_i

```
Initialize η_SE = 0, α_i = 0;
Calculate β_1 and β_2 using (45);
Calculate value range of α_i using (21) and C_56d, expressed as
  (α_i)_min ≤ α_i ≤ (α_i)_max ;
Calculate the iteration accuracy, expressed as:
  Δ(α_1) = ((α_1)_max − (α_1)_min)/n, Δ(α_2) = ((α_2)_max − (α_2)_min)/n;
for j = 0; j ≤ n; j ++ do
    for k = 0; k ≤ n; k ++ do
        ᾱ_1 ← (α_1)_min + jΔ(α_1);
        ᾱ_2 ← (α_2)_min + kΔ(α_2);
        Calculate ᾱ_3 using C_57c;
        if α_3 ∈ [(α_3)_min, (α_3)_max] and α_i ≥ 0.1 then
            Calculate η̄_SE using (39);
            if η̄_SE ≥ η_SE then η_SE ← η̄_SE;
            α_i ← ᾱ_i;
            else α_i ← α_i;
        else
            do state 14;
```

where $\mathrm{C}_{57\mathrm{c}}$ is derived by substituting (51) in $\mathrm{C}_{56\mathrm{c}}$ and σ^2 is normalized to unity. Since α_i is a multiplicative dimming factor per layer in DTH-OFDM, for small α_i it would be challenging to recover the transmitted signal with AGWN. Therefore, we have set a constraint to α_i as $|\alpha_i| \geq 0.1$ in the following Algorithm 1. Finally, the solutions for (P2.2) are determined using the global search in Algorithm 1.

3) Dimming Stage III ($\eta_H < \eta < 1$): For this, we consider it as an asymmetric stage of the dimming stage I by setting $I_{\mathrm{bias}} = I_{\mathrm{H}}$ and α_i being negative. Thus, the constrained joint dimming control and optimal allocation problem can be formulated as

$$\begin{aligned} (\mathrm{P3}): \quad & \min_{\beta_1,\beta_2} \quad P_{b,\mathrm{THO}} \\ & \text{s.t.} \quad \alpha_i < 0, \ \ i = 1,2,3, && \text{(58a)} \\ & \qquad I_{\mathrm{bias}} = I_H, && \text{(58b)} \\ & \text{and} \quad \mathrm{C}_{51}, \mathrm{C}_{53}. \end{aligned}$$

Similar to the dimming control as stage I, we have $\alpha_1 = \alpha_2 = \alpha_3 = -\alpha$, which is given by

$$\alpha = \frac{2\sqrt{2\pi}(1-\eta)}{\sqrt{2} - 1 + \frac{1}{\beta_1}}, \tag{59}$$

and $\eta_H = 1 - \eta_L$.

In summary, we can jointly describe the three dimming stages using pseudocode as shown in Algorithm 2.

VI. Numerical Results

In this section, numerical results are provided by Monte-Carlo simulation to evaluate and validate the proposed DTH-OFDM scheme with joint dimming and communication functions.

Fig. 6 first shows the dimming level η as a function of I_{bias} for DTH-OFDM under the different α_i orders, where the scaling factors γ_i are set as 2, 3, 4 and 5, respectively. The

Algorithm 2: Joint dimming control and optimal power allocation for the proposed DTH-OFDM

Input: target illumination level η, M_1, M_2, I_L, I_H, σ^2
Output: α_i, I_{bias}
Calculate β_1 and β_2 using (45);
Calculate η_L using (55);
$\eta_H = 1 - \eta_L$;
if $0 < \eta < \eta_L$ **then**
    $I_{\text{bias}} \leftarrow I_L$;
    Calculate α_i using (54);
else if $\eta_L \leq \eta \leq \eta_H$ **then**
    $I_{\text{bias}} \leftarrow \eta$;
    Calculate α_i using Algorithm 1;
else
    $I_{\text{bias}} \leftarrow I_H$;
    Calculate α_i using (59);

plots illustrate a linear increase of η with I_{bias}. For example, in Fig. 6(a), the adjustable range of η has increased from [0.6, 1] to [0.24, 1] for γ_i of 2 and 5, respectively. Note, γ_i adjustment is achieved by changing α_i. On the other hand for a fixed I_{bias}, η can changed by adjusting α_i. Note, the same pattern can also be seen in Figs. 6(b)-(d). However, in real dimming applications a single parameter-based dimming adjustment will not meet the requirement for a wide dimming range, which is achieved by means of jointly adjusting α_i and I_{bias} in the proposed scheme.

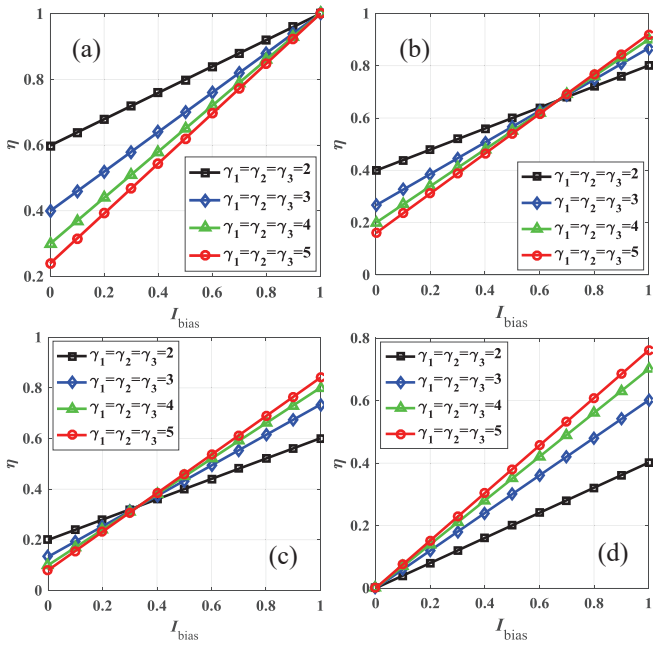

Fig. 6. The dimming level η as a function of I_{bias} with various scaling factors γ_i in DTH-OFDM. (a) Dimming factors $\alpha_i > 0$; (b) Dimming factors $\alpha_1, \alpha_2 > 0$, $\alpha_3 < 0$; (c) Dimming factors $\alpha_1 > 0$, $\alpha_2, \alpha_3 < 0$; (d) Dimming factors $\alpha_i < 0$.

The average BER comparison for various dimmable schemes are then presented in Fig. 7, where the total number of SCs $N = 512$ and the LED nonlinearity has not been taken into account. The dimming level values of 0.1 (stage I), 0.3 (stage II) and 0.5 are representative for DTH-OFDM because the dimming range are symmetric about $\eta = 0.5$ in DTH-OFDM. Note that in RPO-OFDM and HLACO-OFDM schemes, the BER performance under different dimming target can be independent with η due to its inherent characteristic of dimming mechanism. Obviously, the proposed DTH-OFDM can reach the best BER performance when $\eta = 0.3$, about 2 and 4 dB SNR gain under the BER of 10^{-4} compared with RPO-OFDM and HLACO-OFDM, respectively. In addition, the SEs of DTH-OFDM and HLACO-OFDM are 1.75 times of RPO-OFDM, which shows the drawback of RPO-OFDM. On the other hand, the BER performance of DTH-OFDM is also better than THO-OFDM when $\eta = 0.3$ and 0.5, since it employs the convex optimization to tackle the optical power allocation during triple-layers of THO-OFDM.

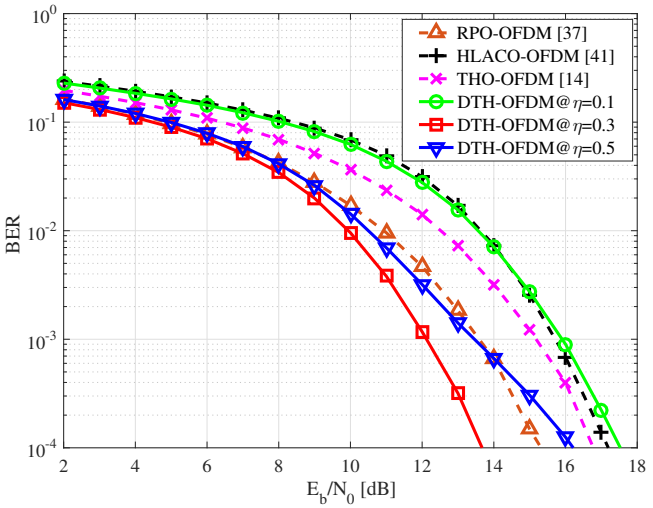

Fig. 7. BER comparisons between the proposed DTH-OFDM with various dimming level η and the RPO-OFDM, HLACO-OFDM with 3 layers and THO-OFDM, where the modulation formats for ACO-OFDM and PAM-DMT are set as 16QAM and 4PAM.

Afterwards, the average BER performance of the DTH-OFDM with 16QAM and 4 PAM for different dimming levels η from 0.05 to 0.95 in three dimming stages is further depicted in Fig. 8, where $\frac{E_b}{N_0} = 14$ and 16 dB. Taking Fig. 8(a) for example, blue dotted lines of Fig. 8(c), (d) and (e) are the BER plots for the case with no LED nonlinearity at the dimming stages I, II and III, respectively, which symmetry at $\eta = 0.5$. Note, the BER plots of (c) and (e) are the same since the dimming stages I and III are antisymmetric. However, at stage II the polarities of α_i are changeable, which means that part of time-domain signal amplitude in DTH-OFDM could be canceled thus leading to a wider adjustment range of each layer, i.e. α_i. Since the objective function in dimming stage II is to maximize η_{SE} under the constraints $\text{C}_{57\text{b}}$ and $\text{C}_{57\text{c}}$, each layer signal enable to achieve bigger α_i compared with stage I and III, which means that it fully exploit the dynamic range of LED and improve the effective SNR at the receiver [39]. Therefore, the average BER performance could be better in stage II.

The red solid line plots of Fig. 8(f), (g) and (h) denote the BER performance for dimming stages I, II and III, respectively with LED nonlinearity when $I_L = 0$ and $I_H = 1$. Since the exceeded part of current signal would be clipped at the

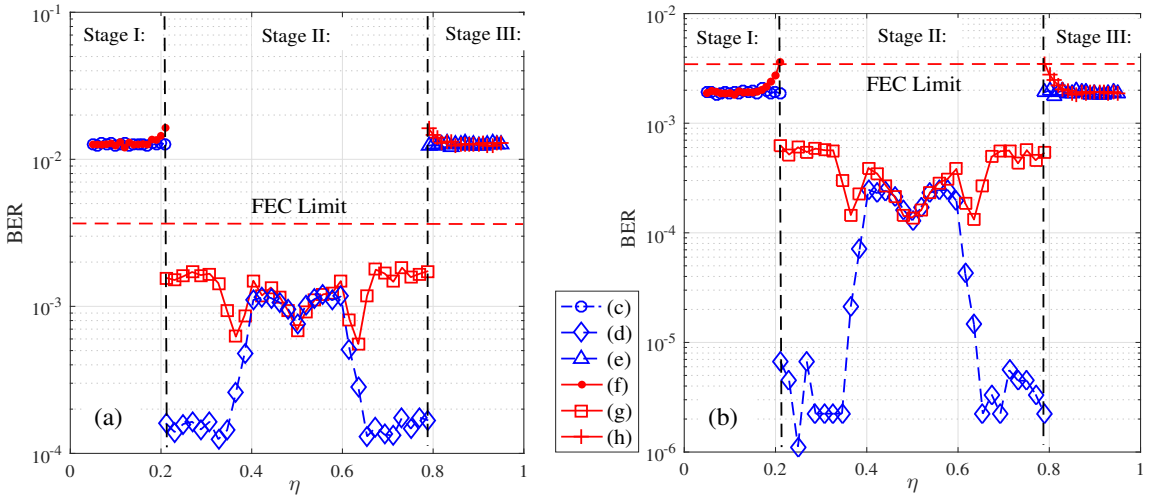

Fig. 8. BER performance of the proposed DTH-OFDM as a function of η using 16QAM and 4PAM when (a) $\frac{E_b}{N_0} = 14$ dB and (b) $\frac{E_b}{N_0} = 16$ dB, where (c)-(e) represent the different dimming stages without considering LED nonlinearity while (f)-(h) represent that considering LED nonlinearity.

threshold value of I_L and I_H, the DTH-OFDM signal in the region close to the dimming stages margins would experience clipping-induced distortion due to the LED nonlinearity. For example, for the dimming stage I, the probability of clipping increases with η, thus resulting in deterioration of BER performance as α_i increases. The same can be said to the other two dimming stages of II and III. Note, for DTH-OFDM VLC in Fig. 8(b), (i) considering the LED nonlinearity the average BER is still lower than the forward error correction (FEC) limit (BER $= 3.8 \times 10^{-3}$ and the redundancy ratio of 7%) for an arbitrary η; (ii) it offers lower BER (i.e., a good nonlinearity tolerance) for $\eta < 0.15$, $0.4 < \eta < 0.6$ and $\eta > 0.85$; and (iii) it shows higher BER for the case for LED nonlinearity for $0.2 < \eta < 0.4$ and $0.6 < \eta < 0.8$.

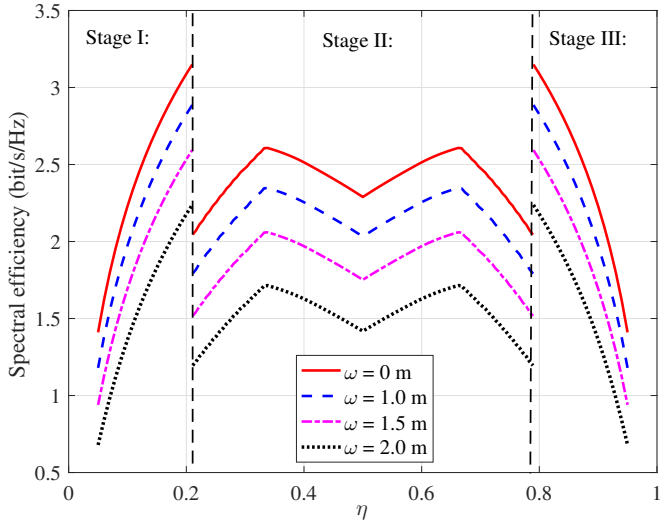

Fig. 9. Achievable spectral efficiency of DTH-OFDM for indoor VLC as a function of η with various horizontal distance w.

In indoor VLC, both η and channel parameters will also affect the link performance. Fig. 9 shows the SE versus η for the three dimming stages with a range of w when σ^2 is normalized to unity, and N_0 of 10^{-20}. All other parameters used are the same as those listed in Table II. As can be seen, the SE plots are symmetric at $\eta = 0.5$ for all values of w, and decrease with the increasing w for three dimming stages due to reduced received optical power levels along the LOS path between LED and PD. Specifically, for the dimming stages I and III, the increase in SE is due to higher α_i, whereas for the dimming stage II, the average SE is almost contrast for all values of w. Note, the objective function in dimming stage II is to maximize SE and minimize the average BER under constraints, where the SE plots are relatively high while maintaining the lower BER performance, see Fig. 8.

VII. Conclusion

In this paper, a joint dimming control and optimal power allocation scheme for DTH-OFDM VLC was proposed to simultaneously support illumination and data communications in a LOS indoor environment. The transmitted signal structure for DTH-OFDM and a typical LOS channel were modeled. Based on minimized average BER using convex optimization for DTH-OFDM, which shows the global minimum point at (β_1, β_2) = (0.3886, 0.2748) for 16QAM and 4PAM, three dimming stages were formulated and then solved to meet both illumination and data communications requirements. The numerical results showed that, the proposed DTH-OFDM scheme could achieve an arbitrary and continuous dimming level from 0.05 to 0.95 by jointly adjusting the dimming factors α_i and I_{bias}. In addition, we simulated and compared the BER performance for DTH-OFDM with the other typical O-OFDM schemes under a range of η changes and different dimming stages, then results showed an improved tolerance to the LED nonlinearity except for the lower total BER under the FEC limit. Finally, we compared the SE plots as a function of η for a range of horizontal weight w with the highest SE achieved for η of about 0.2 and 0.8.

ACKNOWLEDGMENT

The authors would like to thank the anonymous reviewers for their precious time, valuable comments and inspirational suggestions for improving the paper.

APPENDIX A
PROOF OF PDF OF THE PROPOSED DTH-OFDM

As described in (19), the PDF of two-layer ACO-OFDM signals in DTH-OFDM has been derived. Since we have set α_1 and α_2 are positive for simplification, (19) can be first simplified to

$$\begin{aligned}
&f_{\alpha_1 x_{\mathrm{THO}}^{(1)}}(w)\otimes f_{\alpha_2 x_{\mathrm{THO}}^{(2)}}(w)=\\
&\int_{-\infty}^{\infty}\left[\frac{1}{\sqrt{2\pi}\alpha_1\sigma_1}\exp\left(\frac{-l^2}{2\alpha_1^2\sigma_1^2}\right)u(l)+\frac{1}{2}\delta(l)\right]\times\\
&\left[\frac{1}{\sqrt{2\pi}\alpha_2\sigma_2}\exp\left(\frac{-(w-l)^2}{2\alpha_2^2\sigma_2^2}\right)u(w-l)+\frac{1}{2}\delta(w-l)\right]dl\\
&=\frac{\exp\left(\frac{-w^2}{2\alpha_2^2\sigma_2^2}\right)}{2\pi\alpha_1\alpha_2\sigma_1\sigma_2}\int_0^w\exp\left(\frac{-\alpha_1^2\sigma_1^2-\alpha_2^2\sigma_2^2}{2\alpha_1^2\alpha_2^2\sigma_1^2\sigma_2^2}l^2+\frac{w}{\alpha_2^2\sigma_2^2}l\right)dl\\
&+\frac{1}{2\sqrt{2\pi}}\left[\frac{1}{\alpha_1\sigma_1}\exp(\frac{-w^2}{2\alpha_1^2\sigma_1^2})+\frac{1}{\alpha_2\sigma_2}\exp(\frac{-w^2}{2\alpha_2^2\sigma_2^2})\right]u(w)\\
&+\frac{1}{4}\delta(w).
\end{aligned}\tag{60}$$

After some manipulation and using the integral interval transformation [50], we have

$$\begin{aligned}
\int_0^u\exp(-\frac{x^2}{4\beta}-\gamma x)dx=\sqrt{\pi\beta}\exp(\beta\gamma^2)\\
\times\left[Q\left(\gamma\sqrt{\beta}\right)-Q\left(\gamma\sqrt{\beta}+\frac{u}{2\sqrt{\beta}}\right)\right],
\end{aligned}\tag{61}$$

Substituting (61) into (60) gives

$$\begin{aligned}
&f_{\alpha_1 x_{\mathrm{THO}}^{(1)}}(w)\otimes f_{\alpha_2 x_{\mathrm{THO}}^{(2)}}(w)=\\
&=\frac{1}{\sqrt{2\pi(\alpha_1^2\sigma_1^2+\alpha_2^2\sigma_2^2)}}\exp\left(-\frac{w^2}{2(\alpha_1^2\sigma_1^2+\alpha_2^2\sigma_2^2)}\right)\times\\
&\left[Q\left(-\frac{\alpha_1\sigma_1 w}{\alpha_2\sigma_2\sqrt{\alpha_1^2\sigma_1^2+\alpha_2^2\sigma_2^2}}\right)-Q\left(-\frac{\alpha_2\sigma_2 w}{\alpha_1\sigma_1\sqrt{\alpha_1^2\sigma_1^2+\alpha_2^2\sigma_2^2}}\right)\right]\\
&+\frac{1}{2\sqrt{2\pi}}\left[\frac{1}{\alpha_1\sigma_1}\exp(\frac{-w^2}{2\alpha_1^2\sigma_1^2})+\frac{1}{\alpha_2\sigma_2}\exp(\frac{-w^2}{2\alpha_2^2\sigma_2^2})\right]u(w)\\
&+\frac{1}{4}\delta(w),
\end{aligned}\tag{62}$$

where we have set $\beta=\alpha_1^2\sigma_1^2\alpha_2^2\sigma_2^2/(2\alpha_1^2\sigma_1^2+2\alpha_2^2\sigma_2^2)$ and $\gamma=-w/\alpha_2^2\sigma_2^2$.

Similarly, we can further derive the PDF of DTH-OFDM as the follows, where α_1, α_2, and α_3 are also supposed to be positive

$$\begin{aligned}
&f_{x_{\mathrm{DTH}}}(w)=f_{\alpha_1 x_{\mathrm{THO}}^{(1)}}(w)\otimes f_{\alpha_2 x_{\mathrm{THO}}^{(2)}}(w)\otimes f_{\alpha_3 x_{\mathrm{THO}}^{(3)}}(w)\\
&=\frac{u(w)}{4\sqrt{2\pi(\alpha_1^2\sigma_1^2+\alpha_2^2\sigma_2^2)}}\exp\left(-\frac{w^2}{2(\alpha_1^2\sigma_1^2+\alpha_2^2\sigma_2^2)}\right)\times\\
&\left[Q\left(-\frac{\alpha_2\sigma_2 w}{\alpha_1\sigma_1\sqrt{\alpha_1^2\sigma_1^2+\alpha_2^2\sigma_2^2}}\right)-Q\left(-\frac{\alpha_1\sigma_1 w}{\alpha_2\sigma_2\sqrt{\alpha_1^2\sigma_1^2+\alpha_2^2\sigma_2^2}}\right)\right]\\
&+\frac{u(w)}{4\sqrt{2\pi(\alpha_1^2\sigma_1^2+\alpha_3^2\sigma_3^2)}}\exp\left(-\frac{w^2}{2(\alpha_1^2\sigma_1^2+\alpha_3^2\sigma_3^2)}\right)\times\\
&\left[Q\left(-\frac{\alpha_3\sigma_3 w}{\alpha_1\sigma_1\sqrt{\alpha_1^2\sigma_1^2+\alpha_3^2\sigma_3^2}}\right)-Q\left(-\frac{\alpha_1\sigma_1 w}{\alpha_3\sigma_3\sqrt{\alpha_1^2\sigma_1^2+\alpha_3^2\sigma_3^2}}\right)\right]\\
&+\frac{u(w)}{4\sqrt{2\pi(\alpha_2^2\sigma_2^2+\alpha_3^2\sigma_3^2)}}\exp\left(-\frac{w^2}{2(\alpha_2^2\sigma_2^2+\alpha_3^2\sigma_3^2)}\right)\times\\
&\left[Q\left(-\frac{\alpha_3\sigma_3 w}{\alpha_2\sigma_2\sqrt{\alpha_2^2\sigma_2^2+\alpha_3^2\sigma_3^2}}\right)-Q\left(-\frac{\alpha_2\sigma_2 w}{\alpha_3\sigma_3\sqrt{\alpha_2^2\sigma_2^2+\alpha_3^2\sigma_3^2}}\right)\right]\\
&+\frac{u(w)}{4\sqrt{2\pi}}\left[\frac{\exp(\frac{-w^2}{2\alpha_1^2\sigma_1^2})}{\alpha_1\sigma_1}+\frac{\exp(\frac{-w^2}{2\alpha_2^2\sigma_2^2})}{\alpha_2\sigma_2}+\frac{\exp(\frac{-w^2}{2\alpha_3^2\sigma_3^2})}{\alpha_3\sigma_3}\right]+\\
&\iint\exp\left(\frac{-(w-l-v)^2}{2\alpha_1^2\sigma_1^2}-\frac{l^2}{2\alpha_2^2\sigma_2^2}-\frac{v^2}{2\alpha_3^2\sigma_3^2}\right)u(w-l-v)u(l)u(v)dldv\\
&\times\frac{1}{2\pi\sqrt{2\pi}\alpha_1\sigma_1\alpha_2\sigma_2\alpha_3\sigma_3}+\frac{1}{8}\delta(w).
\end{aligned}\tag{63}$$

APPENDIX B
PROOF OF THE CONVEXITY OF AVERAGE BER $P_{b,\mathrm{THO}}$

For proving the convexity of $P_{b,\mathrm{THO}}$, define its independent variables is in a closed region, which is represented as $D=\{(\beta_1,\beta_2)|\beta_1\in(0,1),\beta_2\in(0,1)\}$. Here, we define $A=\frac{\partial^2 P_{b,\mathrm{THO}}}{\partial\beta_1^2}$, $B=\frac{\partial^2 P_{b,\mathrm{THO}}}{\partial\beta_1\partial\beta_2}$ and $C=\frac{\partial^2 P_{b,\mathrm{THO}}}{\partial\beta_2^2}$, respectively. According to (43), we have

$$\begin{aligned}
A=&\frac{N(\sqrt{M_1}-1)\beta_1}{\lambda\sqrt{2\pi M_1}}\left[\frac{3\pi}{(M_1-1)N_0}\right]^{\frac{3}{2}}\exp\left[\frac{-3\pi\beta_1^2}{2(M_1-1)N_0}\right]+\\
&\frac{(N-8)(M_2-1)(1-\beta_1-\beta_2)}{4\sqrt{2\pi}\lambda M_2}\left[\frac{6\pi}{(M_2^2-1)N_0}\right]^{\frac{3}{2}}\exp\left[\frac{-3\pi(1-\beta_1-\beta_2)^2}{(M_2^2-1)N_0}\right],
\end{aligned}\tag{64}$$

$$\begin{aligned}
B=&\frac{(N-8)(M_2-1)(1-\beta_1-\beta_2)}{4\sqrt{2\pi}\lambda M_2}\left[\frac{6\pi}{(M_2^2-1)N_0}\right]^{\frac{3}{2}}\\
&\times\exp\left[\frac{-3\pi(1-\beta_1-\beta_2)^2}{(M_2^2-1)N_0}\right],
\end{aligned}\tag{65}$$

$$\begin{aligned}
C=&\frac{N(\sqrt{M_1}-1)\beta_2}{\lambda\sqrt{2\pi M_1}}\left[\frac{3\pi}{(M_1-1)N_0}\right]^{\frac{3}{2}}\exp\left[\frac{-3\pi\beta_2^2}{2(M_1-1)N_0}\right]+\\
&\frac{(N-8)(M_2-1)(1-\beta_1-\beta_2)}{4\sqrt{2\pi}\lambda M_2}\left[\frac{6\pi}{(M_2^2-1)N_0}\right]^{\frac{3}{2}}\exp\left[\frac{-3\pi(1-\beta_1-\beta_2)^2}{(M_2^2-1)N_0}\right].
\end{aligned}\tag{66}$$

Then, we can calculate $AC-B^2$, which is given as (67) in the top of next page. According to the above (64)-(67), we can conclude that the second-order partial derivative A,

$$
\begin{aligned}
AC-B^2 = {} & \frac{N^2(\sqrt{M_1}-1)^2\beta_1\beta_2}{4\pi\lambda^2 M_1}\exp\left[\frac{-3\pi(\beta_1^2+\beta_2^2)}{2(M_1-1)N_0}\right]\left[\frac{3\pi}{(M_1-1)N_0}\right]^3 \\
& + \frac{N(N-8)(\sqrt{M_1}-1)(M_2-1)\beta_1(1-\beta_1-\beta_2)}{8\pi\lambda^2\sqrt{M_1}M_2}\exp\left[\frac{-3\pi\beta_1^2}{2(M_1-1)N_0}-\frac{3\pi(1-\beta_1-\beta_2)^2}{(M_2^2-1)N_0}\right]\left[\frac{3\pi}{(M_1-1)N_0}\right]^{\frac{3}{2}}\left[\frac{6\pi}{(M_2^2-1)N_0}\right]^{\frac{3}{2}} \\
& + \frac{N(N-8)(\sqrt{M_1}-1)(M_2-1)\beta_2(1-\beta_1-\beta_2)}{16\pi\lambda^2\sqrt{M_1}M_2}\exp\left[\frac{-3\pi\beta_2^2}{2(M_1-1)N_0}-\frac{3\pi(1-\beta_1-\beta_2)^2}{(M_2^2-1)N_0}\right]\left[\frac{3\pi}{(M_1-1)N_0}\right]^{\frac{3}{2}}\left[\frac{6\pi}{(M_2^2-1)N_0}\right]^{\frac{3}{2}}.
\end{aligned} \tag{67}
$$

B and C of $P_{b,\mathrm{THO}}$ are continuous in the closed region D. Besides, $(1-\beta_1-\beta_2)$ in (64)-(66) denotes the proportion of optical power allocated to layer 3 in the THO-OFDM, which is obviously more than zero, i.e., $1-\beta_1-\beta_2>0$. Therefore, we can conclude that $B>0$ and $AC-B^2>0$, which indicates that $P_{b,\mathrm{THO}}$ is a convex function according to the necessary and sufficient condition that determine the convexity of a function.

REFERENCES

[1] Z. Ghassemlooy, S. Arnon, M. Uysal, Z. Xu, and J. Cheng, "Emerging optical wireless communications-advances and challenges," *IEEE J. Sel. Areas Commun.*, vol. 33, no. 9, pp. 1738-1749, Sep. 2015.

[2] H. Elayan, O. Amin, B. Shihada, R. M. Shubair and M. Alouini, "Terahertz Band: The Last Piece of RF Spectrum Puzzle for Communication Systems," *IEEE Open Journal of the Communications Society*, vol. 1, pp. 1-32, 2020.

[3] Yang, Y., Yamagami, Y., Yu, X. et al, "Terahertz topological photonics for on-chip communication," *Nat. Photon.*, vol. 14, pp. 446–451, 2020.

[4] N. Chi, H. Haas, M. Kavehrad, T. D. Little, and X.-L. Huang, "Visible light communications: Demand factors, beneits and opportunities," *IEEE Wireless Commun.*, vol. 22, no. 2, pp. 5-7, Apr. 2015.

[5] L. E. M. Matheus, A. B. Vieira, L. F. M. Vieira, M. A. M. Vieira and O. Gnawali, "Visible Light Communication: Concepts, Applications and Challenges," *IEEE Commun. Surv. Tutor.*, vol. 21, no. 4, pp. 3204-3237, 2019.

[6] K. Yoshida, P. P. Manousiadis, R. Bian, Z. Chen, C. Murawski, M. C. Gather, H. Haas, G. A. Turnbull and I. D. W. Samuel, "245 mhz bandwidth organic light-emitting diodes used in a gigabit optical wireless data link," *Nature Commun.*, vol. 11, no. 1, 2020.

[7] A. Minotto, P. A. Haigh, Ł. G. Łukasiewicz, E. Lunedei, D. T. Gryko, I. Darwazeh, and F. Cacialli,"Visible light communication with efficient far-red/near-infrared polymer light-emitting diodes," *Light-Sci. Appl.*, vol. 9, no. 1, pp. 1-11, 2020.

[8] M. Ayyash, H. Elgala, A. Khreishah, V. Jungnickel, T. Little, S. H. Shao, M. Rahaim, D. Schulz, J. Hilt and R. Freund, "Coexistence of WiFi and LiFi toward 5G: concepts, opportunities, and challenges," *IEEE Commun. Mag.*, vol. 54, no. 2, pp. 64-71, Feb. 2016.

[9] J. Gancarz, H. Elgala, and T. D. C. Little, "Impact of lighting requirements on VLC systems," *IEEE Commun. Mag.*, vol. 51, no. 12, pp. 34–41, Dec. 2013.

[10] J. K. Kwon, "Inverse source coding for dimming in visible light communications using NRZ-OOK on reliable links," *IEEE Photon. Technol. Lett.*, vol. 22, no. 19, pp. 1455–1457, Oct. 2010.

[11] M. Noshad and M. Brandt-Pearce, "Application of expurgated PPM to indoor visible light communications—Part I: Single-user systems," *J. Lightw. Technol.*, vol. 32, no. 5, pp. 875–882, Mar. 2014.

[12] L.-Y. Wei, C.-W. Hsu, C.-W. Chow, and C.-H. Yeh, "40-Gbit/s Visible Light Communication using Polarization- Multiplexed R/G/B Laser Diodes with 2-m Free-Space Transmission," *Optical Fiber Communication Conference (OFC)*, 2019.

[13] J. Armstrong, "OFDM for optical communications," *J. Lightw. Technol.*, vol. 27, no. 3, pp. 189-204, Feb., 2009.

[14] T. Zhang, H. Ji, Z. Ghassemlooy, X. Tang, B. Lin and S. Qiao, "Spectrum-Efficient Triple-Layer Hybrid Optical OFDM for IM/DD-Based Optical Wireless Communications," *IEEE Access*, vol. 8, pp. 10352-10362, Jan. 2020.

[15] P. A. Haigh, P. Chvojka, Z. Ghassemlooy, S. Zvanovec, and I. Darwazeh, "Visible light communications: multi-band super-Nyquist CAP modulation," *Opt. Express*, 27, pp. 8912-8919, 2019.

[16] Y. Yapıcı and İ. Güvenç, "NOMA for VLC Downlink Transmission With Random Receiver Orientation," *IEEE Trans. Comm.*, vol. 67, no. 8, pp. 5558-5573, Aug. 2019.

[17] J. B. Carruthers and J. M. Kahn, "Multiple-subcarrier modulation for nondirected wireless infrared communication," *IEEE J. Sel. Areas Commun.*, vol. 14, pp. 538–546, Apr. 1996.

[18] J. Armstrong and A. J. Lowery, "Power efficient optical OFDM," *Electron. Lett.*, vol. 42, no. 6, pp. 370–372, Mar. 2006.

[19] S. Lee, S. Randel, F. Breyer, and A. Koonen, "PAM-DMT for intensity-modulated and direct-detection optical communication systems," *IEEE Photon. Technol. Lett.*, vol. 21, no. 23, pp. 1749-1751, Dec. 2009.

[20] S. D. Dissanayake, K. Panta and J. Armstrong, "A novel technique to simultaneously transmit ACO-OFDM and DCO-OFDM in IM/DD systems," *2011 IEEE GLOBECOM Workshops (GC Wkshps)*, Houston, TX, 2011, pp. 782-786.

[21] B. Ranjha and M. Kavehrad, "Hybrid asymmetrically clipped OFDM-based IM/DD optical wireless system," *IEEE J. Opt. Commun. Netw.*, vol. 6, no. 4, pp. 387–396, Apr. 2014.

[22] R. Bai, Q. Wang and Z. Wang, "Asymmetrically Clipped Absolute Value Optical OFDM for Intensity-Modulated Direct-Detection Systems," *J. Lightw. Technol.*, vol. 35, no. 17, pp. 3680-3691, Sept. 2017.

[23] B. L. Li, S. Feng, and W. Xu, "Spectrum-efficient hybrid PAM-DMT for intensity-modulated optical wireless communication," *Opt. Express* vol. 28, no. 9, 2020.

[24] P. Chvojka, A. Burton, P. Pesek, X. Li, Z. Ghassemlooy, S. Zvanovec, and P. A. Haigh, "Visible light communications: increasing data rates with polarization division multiplexing," *Opt. Lett.* vol. 45, pp. 2977-2980, 2020.

[25] D. Tsonev and H. Haas, "Avoiding spectral efficiency loss in unipolar OFDM for optical wireless communication," *IEEE Int. Conf. Commun., (ICC)*, Jun. 2014, pp. 3336–3341.

[26] Q. Wang, C. Qian, X. Guo, Z. Wang, D. G. Cunningham, and I. H. White, "Layered ACO-OFDM for intensity-modulated direct-detection optical wireless transmission," *Opt. Express*, vol. 23, no. 9, pp. 12382–12393, May 2015.

[27] R. Bai and S. Hranilovic, "Absolute Value Layered ACO-OFDM for Intensity-Modulated Optical Wireless Channels," *IEEE Trans. Commun.*, vol. 68, no. 11, pp. 7098-7110, Nov. 2020.

[28] M. S. Islim and H. Haas, "Augmenting the spectral efficiency of enhanced PAM-DMT-based optical wireless communications," *Opt. Express* vol. 24, no. 11, pp. 11932–11949, 2016.

[29] H. Ji, B. Lin, X. Tang, and J. Xu, "Triple-layer hybrid optical OFDM scheme for passive optical network," *Opt. Commun.* pp. 125622, Feb. 2020.

[30] S. Rajagopal, R. D. Roberts and S. Lim, "IEEE 802.15.7 visible light communication: modulation schemes and dimming support," *IEEE Commun. Mag.* vol. 50, no. 3, pp. 72-82, Mar. 2012.

[31] T. Wang, F. Yang, J. Song and Z. Han, "Dimming Techniques of Visible Light Communications for Human-Centric Illumination Networks: State-of-the-Art, Challenges, and Trends," *IEEE Wireless Commun.*, vol. 27, no. 4, pp. 88-95, Aug. 2020.

[32] K. Lee and H. Park, "Modulations for visible light communications with dimming control," *IEEE Photon. Technol. Lett.*, vol. 23, no. 16, pp. 1136–1138, Aug. 2011.

[33] X. You, J. Chen, H. Zheng, and C. Yu, "Efficient data transmission using MPPM dimming control in indoor visible light communication," *IEEE Photon. J.*, vol. 7, no. 4, pp. 1–12, Aug. 2015.

[34] Z. Babar, M. A. Mohd Izhar, H. V. Nguyen, P. Botsinis, D. Alanis, D. Chandra, S. X. Ng, R. G. Maunder, and L. Hanzo, "Unary-Coded Dimming Control Improves ON-OFF Keying Visible Light Communication," *IEEE Trans. Commun.*, vol. 66, no. 1, pp. 255-264, Jan. 2018.

[35] Z. Wang, W.-D. Zhong, C. Yu, J. Chen, C. P. S. Francois, and W. Chen, "Performance of dimming control scheme in visible light communication system," *Opt. Express*, vol. 20, no. 17, pp. 18861–18868, Aug. 2012.
[36] Y. Yang, Z. Zeng, J. Cheng, and C. Guo, "An enhanced DCO-OFDM scheme for dimming control in visible light communication systems," *IEEE Photon. J.*, vol. 8, no. 3, pp. 1–13, Jun. 2016.
[37] H. Elgala and T. D. Little, "Reverse polarity optical-OFDM (RPO-OFDM): Dimming compatible OFDM for gigabit VLC links," *Opt. Express*, vol. 21, no. 20, pp. 24288–24299, Oct. 2013.
[38] Q. Wang, Z. Wang, and L. Dai, "Asymmetrical hybrid optical OFDM for visible light communications with dimming control," *IEEE Photon. Technol. Lett.*, vol. 27, no. 9, pp. 974-977, May 2015.
[39] Q. Wang, Z. Wang, L. Dai, and J. Quan, "Dimmable visible light communications based on multilayer ACO-OFDM," *IEEE Photon. J.*, vol. 8, no. 3, Jun. 2016.
[40] F. Yang and J. Gao, "Dimming Control Scheme With High Power and Spectrum Efficiency for Visible Light Communications," *IEEE Photon. J.*, vol. 9, no. 1, pp. 1-12, Feb. 2017.
[41] Y. Sun, F. Yang and J. Gao, "Novel Dimmable Visible Light Communication Approach Based on Hybrid LACO-OFDM," *J. Lightw. Technol.*, vol. 36, no. 20, pp. 4942-4951, Oct. 2018.
[42] X. Huang, F. Yang, X. Liu, H. Zhang, J. Ye and J. Song, "Subcarrier and Power Allocations for Dimmable Enhanced ADO-OFDM With Iterative Interference Cancellation," *IEEE Access*, vol. 7, pp. 28422-28435, 2019.
[43] X. Zhang, Z. Babar, P. Petropoulos, H. Haas and L. Hanzo. "The Evolution of Optical OFDM," *IEEE Commun. Surv. Tutor.*, Mar. 2021.
[44] R. Mesleh, H. Elgala, and H. Haas, "LED nonlinearity mitigation techniques in optical wireless OFDM communication systems," *IEEE/OSA J. Opt. Commun. Netw.*, vol. 4, no. 11, pp. 865-875, Nov. 2012.
[45] Y. Sun, F. Yang and L. Cheng, "An Overview of OFDM-Based Visible Light Communication Systems From the Perspective of Energy Efficiency Versus Spectral Efficiency," *IEEE Access*, vol. 6, pp. 60824-60833, 2018.
[46] Y. Sun, F. Yang and J. Gao, "Comparison of Hybrid Optical Modulation Schemes for Visible Light Communication," *IEEE Photon. J.*, vol. 9, no. 3, pp. 1-13, Jun. 2017.
[47] K. Cho and D. Yoon, "On the general BER expression of one- and two-dimensional amplitude modulations," *IEEE Trans. Commun.*, vol. 50, no. 7, pp. 1074-1080, Jul. 2002.
[48] S. D. Dissanayake and J. Armstrong, "Comparison of ACO-OFDM, DCO-OFDM and ADO-OFDM in IM/DD Systems," *J. Lightw. Technol.*, vol. 31, no. 7, pp. 1063-1072, Apr. 2013.
[49] Y. Sun, F. Yang and J. Gao, "Near-Optimal Power Allocation and Layer Assignment for LACO-OFDM in Visible Light Communication," *GLOBECOM 2017 IEEE Global Commun. Conf.*, Singapore, 2017, pp. 1-6.
[50] I. S. Gradshteyn and I. M. Ryzhik, "Table of Integrals, Series, and Products," New York, NY, USA: Academic, 2014.

HAN JI received the B.Eng. degree in Engineering Institute from Huaqiao University, Quanzhou, China, in 2018. He is currently pursuing the M.Eng. degree of Electronics and Communication Engineering, in School of Physics from Northeast Normal University, Changchun, China. From Sep. 2019 to Jan. 2020, he was a student trainee in Quanzhou Institute of Equipment Manufacturing, Haixi Institutes, Chinese Academy of Sciences, China. His current research interests include wireless communications theory and performance optimization for visible light communications and optical fiber network.

TIAN ZHANG received the B.Sc. and the M.Sc. degrees in electronic science and technology from the Changchun University of Science and Technology, Changchun, China, in 2010 and 2013, respectively. From 2015 to 2016, he was a Visiting Ph.D. student with the Optical Communication Research Group (OCRG) at the University of Northumbria upon Tyne, U.K. He received the Ph.D. degree in electronic circuit and systems from State Key Laboratory on Integrated Optoelectronics, College of Electronic Science and Engineering, Jilin University, Changchun, China, in 2017. Since 2017, he has been a Lecturer with the School of Physics, Northeast Normal University, Changchun, China. He has authored over 10 IEEE, OSA, IET, Elsevier journals, and 6 conference papers. His research interests include OFDM modulation and digital signal processing for optical and wireless communications.

SHUANG QIAO received the B.Sc. degree in Department of Physics from Jilin Normal University in 1985. He received the M.Sc. degree in Department of Physics from Northeast Normal University, Changchun, China, in 1990. From 1998 to 2000, he was a foreign postgraduate in Faculty of Science from Osaka Kyoiku University, Osaka, Japan. He received the Ph.D. degree in 2004 and then worked as a post doctor from 2004 to 2006 in Changchun Institute of Optics, Fine Mechanics and Physics, Chinese Academy of Sciences, Changchun, China. Since 2000, he has been a Professor with the School of Physics from Northeast Normal University. His research interests include the fields of nuclear imaging and nuclear signal processing, nuclear tube system, ghost imaging technology, and digital signal processing for wireless communication.

ZABIH GHASSEMLOOY (Fellow, OSA; Fellow, IET; Senior Member, IEEE; Member, ACM), CEng, BSc (Hons.) in EE Engineering, Manchester Metropolitan Univ., (1981), MSc (1984) and PhD (1987) from Manchester Univ., UK. 1987-88 as a Post-Doctoral Research Fellow at City Univ., UK. 1988-2004 joined Sheffield Hallam University, UK, and 2004-14 joined Faculty of Eng. Env., Northumbria University, UK as an Associate Dean Research, and currently is the Head of Optical Communications Research Group. He is a Research Fellow (2016-) and a Distinguished Professor (2015-) at the Chinese Academy of Science. He was the Vice-Chair of EU Cost Action IC1101 (2011-16) and is Vice- Chair of the EU COST Action CA19111 NEWFOCUS (European Network on Future Generation Optical Wireless Communication Technologies, 2020-2024). He has published over 900 papers (360 journals and 8 books), over 100 keynote/invited talks, supervised 10 Research Fellows and 65 PhD students. His research interests are in the areas of optical wireless communications, free space optics, visible light communications, hybrid RF and optical wireless communications. He is the Chief Editor of the British Journal of Applied Science and Technology and the International Journal of Optics and Applications, Associate Editor of a number of international journals, and Co-guest Editor of a number of special issues OWC. He is the Vice-Cahir of OSA Technical Group of Optics in Digital Systems (2018-). He is the Chair of the IEEE Student Branch at Northumbria University, Newcastle (2019-). From 2004-06 he was the IEEE UK/IR Communications Chapter Secretary, the Vice-Chairman (2006-2008), the Chairman (2008-2011), and Chairman of the IET Northumbria Network (Oct 2011-2015).